Haploinsufficiency of the mouse Tshz3 gene leads to kidney defects

Irene Sanchez-Martin, Pedro Magalhães, Parisa Ranjzad, Ahmed Fatmi, Fabrice Richard, Thien Phong Vu Manh, Andrew Saurin, Guylène Feuillet, Colette Denis, Adrian Woolf, et al.

Title

Haploinsufficiency of the mouse *Tshz3* gene leads to kidney defects

Authors

Irene Sanchez-Martin[1], Pedro Magalhães[2], Parisa Ranjzad[3], Ahmed Fatmi[1], Fabrice Richard[1], Thien Phong Vu Manh[4], Andrew J. Saurin[1], Guylène Feuillet[5,6], Colette Denis[5,6], Adrian S. Woolf[3,7], Joost P. Schanstra[5,6], Petra Zürbig[2], Xavier Caubit[1], Laurent Fasano[1,*]

Affiliation

1 Aix Marseille Univ, CNRS, IBDM, UMR7288, Marseille, France

2 Mosaiques Diagnostics GmbH, Hannover, Germany.

3 Division of Cell Matrix Biology and Regenerative Medicine, School of Biological Sciences, Faculty of Biology Medicine and Health, University of Manchester, UK.

4 Aix Marseille Univ, CNRS, INSERM, CIML, Centre d'Immunologie de Marseille-Luminy, Marseille, France.

5 Institut National de la Santé et de la Recherche Médicale (INSERM), U1297, Institut of Cardiovascular and Metabolic Disease, Toulouse, France.

6 Université Toulouse III Paul-Sabatier, Toulouse, France.

7 Royal Manchester Children's Hospital, Manchester University NHS Foundation Trust, Manchester Academic Health Science Centre, Manchester, UK.

*** Correspondence:**

Correspondence should be addressed to Laurent Fasano

Tel: +33491269240

laurent.fasano@univ-amu.fr

Abstract

Renal tract defects and autism spectrum disorder (ASD) deficits represent the phenotypic core of the 19q12 deletion syndrome caused by the loss of one copy of the *TSHZ3* gene. While a proportion of *Tshz3* heterozygous (*Tshz3*$^{+/lacZ}$) mice display ureteral defects, no kidney defects have been reported in these mice. The purpose of this study was to characterize the expression of *Tshz3* in adult kidney as well as the renal consequences of embryonic haploinsufficiency of *Tshz3* by analyzing the morphology and function of *Tshz3* heterozygous adult kidney. Here, we described *Tshz3* expression in the smooth muscle and stromal cells lining the renal pelvis, the papilla and glomerular endothelial cells (GEnCs) of the adult kidney as well as in the proximal nephron tubules in neonatal mice. Histological analysis showed that *Tshz3*$^{+/lacZ}$ adult kidney had an average of 29% fewer glomeruli than wild type kidney. Transmission electron microscopy (TEM) of *Tshz3*$^{+/lacZ}$ glomeruli revealed a reduced thickness of the glomerular basement membrane and a larger foot process width. Compared to wild type, *Tshz3*$^{+/lacZ}$ mice showed lower blood urea, phosphates, magnesium and potassium at 2 months of age. At the molecular level, transcriptome analysis identified differentially expressed genes related to inflammatory processes in *Tshz3*$^{+/lacZ}$ compare to wild type (WT; control) adult kidneys. Lastly, analysis of the urinary peptidome revealed 33 peptides associated with *Tshz3*$^{+/lacZ}$ adult mice. These results provide the first evidence that in the mouse *Tshz3* haploinsufficiency leads to cellular, molecular and functional abnormalities in the adult mouse kidney.

Introduction

Congenital anomalies of the kidneys and urinary tract (CAKUT) are the most common cause of renal failure in children (1). Ureteropelvic junction obstruction (UPJO), the most

common paediatric renal obstructive disorder, has an incidence of 1 in 1000-1500 live births screened by antenatal ultrasound (2). Congenital UPJO is usually caused by the presence of an aperistaltic segment of the ureter, preventing the efficient transport of the urine from the kidney to the bladder. UPJO can result from the decrease in the number of smooth muscle cells, interstitial Cajal-like cells and nerve fibers in the ureteropelvic junction. Therefore, impaired transport of urine can lead to an increase in back-pressure on the kidney, hydronephrosis, and progressive damage to the kidney function (3).

The *TSHZ3* gene (Teashirt zinc-finger homeobox family member 3; also known as *ZNF537*), which encodes a zinc-finger transcription factor, was recently identified as the critical region for a 19q12 deletion syndrome (19q12DS): patients with *TSHZ3* heterozygous deletion show lower (i.e. vesicoureteral reflux grade 2) and upper (i.e. UPJO) urinary tract defects as well as kidney (i.e. hydronephrosis and nephrolithiasis) defects(4).

Tshz3 homozygous mutant mice ($Tshz3^{lacZ/lacZ}$) have been used to explore the pathogenesis of *Tshz3* in UPJO (5, 6). Studies have shown that from embryonic day (E) 12.5 onwards TSHZ3 positive cells are detected in the mouse ureter and the kidney (5). In the embryo, *Tshz3* plays a key role in smooth muscle differentiation by regulating *Myocardin (myocd)* expression and MYOCD activity (5, 6). $Tshz3^{lacZ/lacZ}$ mutant mice die perinatally because of their inability to breathe and display bilateral UPJO and hydronephrosis (5, 7). In comparison, one-fourth of $Tshz3^{+/lacZ}$ heterozygous embryos display a unilateral UPJO and hydronephrosis and about 50% die at birth (5-7). However, the impact of *Tshz3* haploinsufficiency on the postnatal kidneys has never been investigated so far.

Therefore, the main aim of this study was to determine whether *Tshz3* heterozygote mice exhibit kidney defects in order to gain insights on whether haploinsufficiency may help explaining kidney diseases reported in patients with heterozygous deletion of *TSHZ3*.

Results

TSHZ3 expression in adult kidneys.

Previous analyses performed during development indicate that the temporal and spatial distribution of β-galactosidase (ß-gal) protein in *Tshz3*$^{+/lacZ}$ mice faithfully reproduces the expression of *Tshz3*/TSHZ3 (5, 6). Here we used the same approach to characterize the expression of *Tshz3*/TSHZ3 in sections of *Tshz3*$^{+/lacZ}$ adult kidneys. X-Gal staining performed on *Tshz3*$^{+/lacZ}$ adult kidney revealed that *Tshz3* is expressed in the pelvic region and ureter, the papilla, perivascular region and the glomeruli (**Fig. 1A-F**). To further characterize the expression of TSHZ3 in the glomeruli, we performed immunostaining, using glomerular cells markers. These analyses showed that β-gal positive cells were endothelial cell (CD31-positive) but not podocytes (Dachshund 1 positive) or mesangial cells (NG2 positive) (**Fig. 1G-I**). In one-week old postnatal *Tshz3*$^{+/lacZ}$ mouse kidneys, TSHZ3 was detected in the tufts of maturing glomeruli and in nuclei of thin tubule-like structures in the kidney cortex (**Fig. 2A**). Subsets of tubule-like profiles also immunostained for TSHZ3 in the outer medulla and the inner medulla (**Fig. 2A-C**). Comparison with immunostaining patterns for aquaporin-1, uromodulin and calbindin-28 (**Fig. 2D-L**), suggest that thin descending limbs of loops of Henle express TSHZ3 because patterns for this protein and aquaporin-1 are similar in the thin tubules within the inner medulla. In this location, calbinin-28 positive collecting ducts are wider diameter and uromodulin is not detected. The TSHZ3 positive tubules in the cortex and outer medulla may also include the pars recta, or straight section, of the aquaporin-1 positive

proximal tubules. The tubule signals for TSHZ3 appeared attenuated in adult kidneys into which we did not observe any major morphological changes (data not shown).

Double immunostaining for β-gal and Smooth muscle alpha-actin (SMAA) confirmed the expression of TSHZ3 in smooth muscle cells in the pelvic region and in SMA-negative Dachshund 1-positive stromal cells lining the urothelium (**Fig. 3**).

$Tshz3^{+/lacZ}$ mice showed glomerular defects.

Comparison of 8-week-old adult kidney histology revealed a decrease of 28.8% in glomerular density in $Tshz3^{+/lacZ}$ compared to WT (**Fig. 4A, B and supplementary Fig. 4**). The same analysis performed with 40-week-old adult kidneys revealed a 44.2% reduction of glomerular density in $Tshz3^{+/lacZ}$ *vs.* WT. In order to identify glomerular morphological changes in $Tshz3^{+/lacZ}$ mice, we conducted an ultrastructural analysis using transmission electron microscopy (TEM). While this analysis did not identify a significant variation of the proportion of the size of the fenestration and endothelial layer (**Fig. 4C, D**), it revealed a significant reduction of the thickness of the glomerular basement membrane (GBM) in glomeruli of $Tshz3^{+/lacZ}$ mutants (144.2 ± 4.2 nm) compared to WT (155.1 ± 3.32 nm) (**Fig. 4E, F**). TEM analysis also showed that in the $Tshz3^{+/lacZ}$ kidneys the foot processes were effaced, reflected by a foot process width (FPW) of 351.7 ± 5.03 nm, ≈14% larger ($P<0.0001$) than in the WT kidneys (303.4 ± 6.57 nm) (**Fig. 4G, H**).

Blood electrolytes are modified in $Tshz3^{+/lacZ}$ mice.

To characterize the effects of *Tshz3* haploinsufficiency on kidney filtration, we performed biochemical measurements on blood samples and generated biochemical profiles for $Tshz3^{+/lacZ}$ and WT adult mice tested at 58-64 days-of-age. Blood analysis demonstrated that $Tshz3^{+/lacZ}$ mice have significant reduction of the urea ($P<0.013$), phosphates

(P<0.011), magnesium (P<0.014), potassium (P<0.0034) as well as an increased concentration of sodium (*P* <0.012) (**Fig. 5; Table 1a**). We found no significant variation in creatinine concentration in *Tshz3*$^{+/lacZ}$ compared to WT (15.91 ± 1.51 vs. 12.36 ± 2.07 µM/l; P<0.09).

The *Tshz3*$^{+/lacZ}$ adult kidney showed differential expression of genes involved in inflammatory processes.

To identify *Tshz3*-regulated genes in the adult kidney, RNA sequencing analysis was performed with samples extracted from *Tshz3*$^{+/lacZ}$ (n=6) and wild type (WT; controls, n=6) adult mouse kidneys. 97 differentially expressed genes (DEGs) were identified, among which 55 were up-regulated and 42 were down-regulated (adjusted p-value < 0.01) (**Table 1b**). Thereafter, we sought to take advantage of the single-cell transcriptome of mouse glomeruli (8) and adult kidney(9) to identify the cell types in wild type kidneys that expressed the genes differentially expressed in *Tshz3*$^{+/lacZ}$ kidney. This analysis identified 58 genes expressed in podocytes, 31 in mesangial cells, 27 in immune cells, 40 in tubules and 43 in GECs, which might be direct targets of TSHZ3 (**Table 1c**). We also found that some DEGs were shown to be markers of proximal tubules (*Aspdh*, *Snhg11* and *D630029K05Rik*, a long non-coding RNA) or myeloid lineage (*Cd74*, *Gusb*, *H2-Aa*, *H2-Ab1*, *Lyz2*, *Mpeg1* and *Vcam1*), including macrophages and dendritic cells (10).

To characterize the differential expression data and to identify biological changes that occur in *Tshz3*$^{+/lacZ}$ kidneys, we performed different enrichment analyses. As only a few genes showed very strong differential expression, we applied gene set enrichment analysis (GSEA (11, 12)) using a ranked gene list. We chose the updated public genesets available on MSigDB (12) and identified positive enrichment in the kidneys of *Tshz3*$^{+/lacZ}$ adult mice for gene sets related to “interferon-gamma response”, “epithelial to

mesenchymal transition", "inflammatory response" and negative enrichment for genes related to "Oxidative Phosphorylation" and "Xenobiotic Metabolism" (**Table 1d; Supplementary Fig. 1**). Furthermore, ingenuity pathway analysis (IPA) of the DEGs revealed enrichment of cellular processes centered on inflammatory and kidney diseases (**Supplementary Fig. 2A, B**). This analysis showed that the relevant toxicity phenotypes and pathology endpoints associated with the DEGs in *Tshz3*$^{+/lacZ}$ mice were centered on the kidney and identified interferon-gamma (IFNG) as an upstream regulator (**Supplementary Fig. 2B, C**). Moreover, enrichment analysis of pathways and transcription factor using enrichR (13) also identified the "*interferon gamma*" pathway but also "*collagen formation*" and "*extracellular matrix organization*" as significantly enriched in *Tshz3*$^{+/lacZ}$ adult kidneys (**Table 1e**). Interestingly, the ChIP enrichment analysis (ChEA) and a database search revealed that 22 DEGs (21.68%) are direct targets of the transcription factor interferon regulatory factor 8 (IRF8) (**Table 1f**).

Using RT-qPCR we confirmed the DEG status observed by RNA-seq analysis for *Ciita*, *Pld4* (two targets of IRF8), *Tlr7* (IRF8 target that promotes IFNG production (14)) and the proinflammatory *Npy* (**Supplementary Fig. 3**).

Genes differentially expressed in *Tshz3*$^{+/lacZ}$ adult kidney are associated with ASD

To gain insights into *TSHZ3* function, we studied the disease association of the 80 non-ambiguous human orthologs of the mouse DEGs (**Table 1g**). This analysis identified 35/80 genes (43.75%), which were established or putative causes for kidney disorders. Interestingly, 8 of these genes have been also associated with ASD (**Table 1h**).

Identification of *Tshz3*$^{+/LacZ}$-related urinary peptides

Since *Tshz3*$^{+/lacZ}$ mice exhibit dysregulated kidney expression of several genes and altered hematological parameters, we sought to analyze their urinary peptidome. Urine samples

derived from *Tshz3*$^{+/LacZ}$ (n=15) and WT (n=12) were analyzed by capillary electrophoresis coupled to mass spectrometry (CE-MS). Comparison of urinary peptidome profiles led to the identification of 33 peptides that were significantly (adjusted p-value < 0.05) associated with *Tshz3*$^{+/lacZ}$ (**Fig. 6**). Protein fragments from clusterin (CLUS), complement factor D (CFAD), histone H2B type 1-F/J/L (H2B1F), major urinary protein 17 (MUP17), tripeptidyl-peptidase 1 (TPP1) and uromodulin (UMOD), as well as a large number (27) of collagen fragments, were identified (**Table 1i)**. *Tshz3*$^{+/lacZ}$ mice showed a decreased concentration of uromodulin and an increased concentration of peptides from CLUS, CFAD, H2B1F, MUP17 as well as TPP1 fragments. Twelve collagen peptides were in higher abundance and fifteen in lower abundance. As UPJO can lead to significant kidney damage, we compared the identified 33 urinary peptides from mice with those of the CKD273 classifier, a predictive marker of chronic kidney disease (CKD) progression in humans(15). This analysis identified 14 similar (orthologs) human peptides in the CKD273 classifier, most of which were collagen fragments (10 from collagen type I alpha-1 chain and 3 from type III alpha-1 chain). One peptide fragment was from uromodulin.

Discussion

Previously, we reported that in mice and humans, haploinsufficiency of *Tshz3/TSHZ3* results in hydroureter (5, 16) and that individuals with *TSHZ3* heterozygous deletion are at risk to develop kidney diseases (16). However, the expression of *Tshz3* in adult kidney and the morphology of *Tshz3* heterozygous adult kidney have not been investigated before. Herein, we characterized TSHZ3 expression in the adult mouse kidney, in particular in glomeruli where TSHZ3 is specifically expressed in endothelial cells (GEnCs), which is supported by single-cell RNA sequencing analysis (8). Using *Tshz3*$^{+/lacZ}$ heterozygous mice, we have also uncovered a key role for the TSHZ3

transcription factor in controlling the glomerular density and morphology. Notably, we showed that *Tshz3*$^{+/lacZ}$ mice have abnormal blood electrolytes and identified *Tshz3*$^{+/LacZ}$-related urinary peptides. In addition, by coupling transcriptomics with *in silico* analysis, we showed that in kidneys from *Tshz3*$^{+/LacZ}$ mice, the expression of genes associated with inflammatory processes and of renal- and ASD-associated was different from that in WT mice. Combined with our previous reports, our data suggest that the *Tshz3* heterozygous mice constitute a model that replicates many of the corresponding human disease phenotypes.

The GEnCs, together with the glomerular basement membrane (GBM) and the podocytes, constitute the glomerular filtration barrier (GFB), which selectively filtrates the plasma. The GBM derives from the fusion of the basement membranes of both GEnCs and podocytes, and in adult kidney, the GEnCs may contribute to the renewed biosynthesis of the GBM. Because abnormalities in each of the three constituents of the GFB can lead to proteinuria and kidney disease, TEM was used to assess fine structures of the GFB. While TEM analysis revealed no obvious structural phenotype in TSHZ3-expressing GEnCs, it provided evidence that *Tshz3* haploinsufficiency leads to GBM thinning and change in podocyte morphology evidenced by effaced foot process. Interestingly, hematuria has been reported in individuals with a thin GBM (17) but we did not observe blood staining (macrohematuria) in the urine samples from *Tshz3* heterozygous mice. In the future, it would be interesting to investigate whether these mice have microhematuria. At present, the primary cause of the structural defects observed in the GBM and the podocytes remains unknown. However, since communication between intraglomerular cells is required for proper development and maintenance of the GFB (18), GBM thinning and larger FPW might be the direct or indirect consequences of an abnormal cross-talk between the TSHZ3-positive GEnCs and other glomerular cells. Furthermore, *Tshz3* may

be transiently expressed in glomerular cell lineages. Nevertheless, the comparison of the urinary peptidome of *Tshz3*$^{+/lacZ}$ and WT adult led to the identification of 27 collagen and 6 non-collagen peptides associated with *Tshz3*$^{+/lacZ}$ mice. Among the collagen fragments displaying a deregulation (e.g. 12 increased or 15 decreased), we identified thirteen collagen fragments that overlap the CKD273 classifier that might be indicative of the development of fibrosis (19, 20). As previously suggested (21), the fragments overlapping the human CKD273 classifier could be used as biomarkers to assess renal function in patients with *TSHZ3* heterozygous deletion. Interestingly, our analysis of urinary peptides also revealed an under-representation of a MUP17 peptide in *Tshz3*$^{+/lacZ}$ mice. The MUP17 protein is predominantly expressed in males and dominant males significantly increased the secretion of MUP17 in social conditions (22, 23). In the future, it would be interesting to study the relationship between variations in the level of MUP17 and the severity of the social behavior deficit observed in *Tshz3*$^{+/lacZ}$ mice. To further evaluate renal function, we performed biochemical measurements on blood samples and generated biochemistry profiles. This analysis identified a significantly reduced concentration for urea, phosphates, magnesium and potassium in *Tshz3*$^{+/lacZ}$ mice. Reduced serum urea is less frequent and usually of less clinical significance than increased serum urea (24, 25). The lower plasma magnesium (hypomagnesaemia), phosphate (hypophosphatemia) and potassium (hypokalemia) serum concentration are associated with defective reabsorption/excretion process in the distal nephron (26-28). However, the decrease in potassium concentration in *Tshz3*$^{+/lacZ}$ mice should be viewed with caution since the method of euthanasia had an effect on potassium level (29). In line with this, single-cell transcriptional profiling of the healthy kidney of 4-8 weeks old mice showed expression of *Tshz3* in the proximal tubule, distal convoluted tubule as well as in collecting duct principal and intercalated cells (9) and our immunostaining studies

suggest that *Tshz3* is indeed not only expressed in glomeruli but also, at least in the early post-natal period, in subsets of tubules, most likely the straight section of the proximal tubule and the thin descending limb of the loop of Henle. This segments are respectively implicated in reclaiming substances, including magnesium, from the glomerular ultrafiltrate, and in the mechanism required for urinary concentration in the medulla (30-32). Altogether, our data suggest that *Tshz3* haploinsufficiency might impact different components of the nephron.

To identify pathways that might be altered, we performed RNA-seq analysis and detected 97 statistically significant changes in gene expression in adult kidneys of $Tshz3^{+/lacZ}$ as compared to WT. Based on the results of enrichment analyses, we detected the involvement of inflammation-related pathways such as interferon-gamma. Of note, seven DEGs (*Crym, Ctss, Fasn, Fcgrt, Gabrb3, Lyz2,* and *Vcam1*) were found to be associated with kidney diseases, including renal inflammation, crescentic glomerulonephritis or end-stage renal failure. Interestingly, population-based studies support that autism spectrum disorder (ASD) and kidney disease coexist in several genetic disorders (for review see Table 2 in (33)), suggesting that the same genetic modification can affect neurodevelopment and nephrogenesis. However, because the genetic alterations (deletion or duplication) associated with these disorders often encompass several genes, it is still unclear how these genes contribute to the underlying molecular mechanisms. In this context, the *TSHZ3* gene which associates ASD with a congenital kidney condition is quite unique (4) and our findings that heterozygous deletion of *Tshz3* leads to kidneys defects might be relevant for patients with *TSHZ3* heterozygous deletion. For example, we found a decreased glomerular density that potentially might lead to a reduced glomerular filtration rate (GFR), a defect that was reported in a patient with heterozygous deletion of the *TSHZ3* gene (Table1 in (4)) who required renal transplant

(Table 2 in (34)). However, we did not find that creatinine level was significantly altered in *Tshz3* heterozygous mice but this measurement is not very accurate to estimate the GFR. Therefore, we must be cautious about whether *Tshz3* heterozygous mice have an altered GFR. It is possible to measure GFR in adult mice, although the technology to do so is technically challenging (35). In future, this could be applied to our mouse model. The reduced number of glomeruli also questions about the mechanism leading to this defect. The reduction of the glomerular density could be a secondary defect in a subtle branching defect but it would require a new study to formally validate this hypothesis. We actually do not observe *Tshz3* expression in the ureteric bud-collecting duct epithelial lineage ((5) and this study). On the other hand, we do see *Tshz3* in the interstitial stroma around this epithelial lineage ((5) and this study) and we cannot exclude that there is a defect in the crosstalk between these two compartments (36) in *Tshz3* heterozygous mice. Our results might also provide to be of interest for cognitive defects link to TSHZ3 haploinsufficiency. For now, the role of low plasma concentration of magnesium in ASD is still a matter of debate. While two studies did not find a statistically significant difference in levels of magnesium in children diagnosed ASD (37, 38), two other studies (39, 40) demonstrated lower levels of magnesium in children diagnosed with ASD. So far, *Tshz3* mouse models have been shown to be quite analogous to the clinical problems (i.e. ASD-associated deficits, hydroureter and hydronephrosis) reported in patients with *TSHZ3* heterozygous conditions (4, 5). Our results generate new hypotheses that might lead to further understanding of the clinical problems and to a better diagnosis management of *TSHZ3* patients.

Materials and methods

Mouse strain and genotype

The *Tshz3*$^{+/LacZ}$ mouse line has been described previously (5).

Samples collection and RNAseq

For RNA sequencing, *Tshz3*$^{+/LacZ}$ and wild-type mice kidneys were collected at 60 days-of-age. The mean values for body weight of the *Tshz3*$^{+/LacZ}$ and wild-type were 34.7± 3.9 g (n=6) and 34.6 ± 6.5 g (n=6), respectively. Dissected kidneys were stored in RNAlater solution (Qiagen) and kept frozen at -80 °C until RNA extraction.

Total individual kidney RNA was extracted using anRNeasy Maxi kit75162 Lot.260018727/ Lot.160012031 from Quiagen according to manufacturer's instructions. The integrity of RNA was assessed using a chip-based capillary electrophoresis machine and RNA concentration determined using a full spectrum (220-750nm) spectrophotometer. The quality control of the RNA was additionally checked with RNA 6000 Pico de Agilent Technologies, according to the manufacturer's instructions. To obtain two independent total RNA preparations from the two different conditions (wild type: WT1 & WT2; *Tshz3*$^{+/LacZ}$: HET1 & HET2) we pooled RNA from 3 kidneys per group in the same proportion. The starting material (1µg Total mRNA, dissolved in RNase-, DNase- and protease-free molecular grade water) was sent to GATC (Eurofins) for sequencing (Genome Sequencer Illumina HiSeq).

Sequences (fastq format) were mapped to the mm10 version of the mouse genome to generate Sequence Alignment/Map (SAM/BAM) format. After normalization, analysis of differentially expressed genes (DEGs) was performed using both the Bioconductor (http://www.bioconductor.org) package DESeq/DESeq2 and the package edgeR.

This analysis generated differential expression lists with False Discovery Rates (FDRs), which are derived from p-values corrected for multiple testing using the Benjamini-Hochberg method. 6 files in total were generated: FDR 1%, 10% for both UCSC (transcripts) and ENSEMBL (genes).

EnrichR tool (13) was used to performed enrichment analysis with “pathways”, gene ontology biological processes (GOBP) and transcription factor (ChIP Enrichment Analysis, ChEA). Gene set enrichment analysis (GSEA) was performed using the software provided by the Broad Institute (41, 42) with default parameters and a pre-ranked gene list calculated based on the10 negative $\log_{10}$ of the *P*-value from DESeq2 analysis multiplied by the sign of differential expression.

mRNA extraction, cDNA synthesis and quantitative real-time PCR (RT-qPCR)

Total RNA from adult kidneys of WT and *Tshz3*$^{+/lacZ}$ mice was prepared using a RNeasy Maxi Kit (ref 75162 Qiagen™), and first-strand cDNA was synthesized using a Maxima First Strand cDNA Synthesis Kit with dsDNase (ThermoFisher Scientific™ ref K1671 50). All samples from each experiment were reverse-transcribed at the same time, and real-time PCR was performed on a StepOne+ qPCR detection system (Applied Biosystems™) using Luminaris Color HiGreen High ROX qPCR Master Mix (Thermo Fisher Scientific™ ref K0362). RT-qPCR conditions were as follows: 40 cycles of 95 °C for 15 s and 60 °C for 60 s. Reactions were run in triplicate in three independent experiments. The geometric mean of the housekeeping gene GAPDH was used as an internal control to normalize variability in expression levels, and samples were also normalized to their respective control group. Specificity of reactions was verified by melt curve analysis. Primer sequences used for Sybr qPCR are as follows:

	gene	Primer FW	Primer Rev
1	*Gbp4*	CAGGCTCTACATGGACATGAGG	TGCCTGCAAGATGGAACTCTCG
2	*Ciita*	ACCTTCGTCAGACTGGCGTTGA	GCCATTGTATCACTCAAGGAGGC
3	*Tlr7*	GTGATGCTGTGTGGTTTGTCTGG	CCTTTGTGTGCTCCTGGACCTA
4	*Npy*	TACTCCGCTCTGCGACACTACA	GGCGTTTTCTGTGCTTTCCTTCA
5	*Gapdh*	GTCTCCTGCGACTTCAACAGCA	ACCACCCTGTTGCTGTAGCCGT

Expression data were normalized to controls and the variability in expression levels was analyzed using the $2^{-\Delta\Delta CT}$ method described Livak and Schmittgen (43).

Variables which showed a p-value less than 0.05 in the resulting model were considered to have a significant effect. These statistical analyses were performed by unpaired t-tests with the qbase+ software version 2 (Biogazelle).

Immunological and in situ hybridization analysis

Adult mice were transcardially perfused with phosphate-buffered saline (PBS, 10 mM, pH 7.4), followed by 4% paraformaldehyde (PFA) in PBS under ketamine (150 mg/kg) and xylazine (20 mg/kg) anesthesia. Kidneys were post-fixed in 4% paraformaldehyde (PFA; EMS Lot.160401) for 2 h at 4 °C, cryoprotected with 30% sucrose solution in PBS and frozen (Iso-Pentane RPE524391 Carlo Erba at dry ice temperature). Immunostaining was performed on 12-µm cryosections from tissues embedded in OCT compound. Cryosections were washed with 0.2% Tween/PBS for 15 min and then blocked in 10% goat serum 0.1%/0.1% Tween/PBS for 1 h. Sections were incubated with primary antibodies overnight at 4 °C. Secondary antibodies were incubated 2 h at room temperature, and after several washes, sections were counterstained with DAPI for 10 minutes.

The following primary antibodies were used: anti-β-galactosidase (chicken, 1/1000, ab9361, Abcam; rabbit, 1/1000, Cappel), mouse anti-NG2 (1/100, MAB5384 Millipore), rabbit anti-CD31/Pecam (1/100 MEC13.3, BD Pharmingen) and rabbit anti-DACH11 (1/100, Proteintech 10914-1-AP). Secondary antibodies: Alexa-Fluor-546 goat anti-mouse; Alexa-Fluor-546 donkey anti-rabbit, Alexa-Fluor 488 donkey anti-mouse, Alexa-Fluor-488 donkey anti-chicken. Slides were mounted with Fluoromount-G, Southern Biotech Lot: B0216-N156. Images were acquired using a laser scanning confocal microscope (LSM780; Carl Zeiss) and processed using Adobe Photoshop.

For X-gal staining, kidneys/ureters were dissected from non-perfused animals, kidneys were cut in two according to the sagittal plane, and tissues were fixed for 1 h in 1% PFA. Detection of β-galactosidase activity was done on tissues or on 14-µm cryostat sections incubated in the dark in staining solution at 37 °C. X-gal staining was performed as described (44). Samples were paraffinized after washing in increasing alcohol concentrations (70%, 80%, 90%, 97% and 100%) VWR chemicals for one day and finally with Xylene 33817 (Sigma-Aldrich) for 2 h, and immersed in paraffin Paraplast X-TRA from Sigma at 65 °C. Staining was performed with Hematoxylin (HHS32-1L Lot. 064K4354 Sigma-Aldrich), Eosin (Ht110230-1L Sigma-Aldrich), Trichrome Masson (Lot.17301-V04 Ral Diagnostics).

To characterize the expression of TSHZ3 in the tubules, immunostaining was performed on kidneys of *Tshz3*$^{+/lacZ}$ mice, using renal tracts of normal external appearance (e.g. no hydronephrosis). Paraformaldehyde-fixed kidneys were embedded in paraffin and 4 µm sections were cut, dewaxed and rehydrated. These sections were incubated overnight at 4°C with antibodies raised in rabbits to define nephron segments and collecting ducts, as described (30-32, 45, 46): aquaporin-1 (1:500, Abcam, ab15080), a marker of proximal tubules and the thin descending limb of the loop of Henle; uromodulin (1:200, Santa Cruz, sc-20631), a marker of the thick ascending limb of the loop of Henle; and calbindin-28, a marker of distal tubules of the nephron and also of collecting ducts (1:500, Abcam, ab25085). For immunostaining of TSHZ3, we used an antibody (1:1000) raised in guinea pig, as described (5). Our preliminary experiments showed that this antibody did not work well on paraffin section but was effective on optimal cutting temperature compound (OCT)-embedded frozen sections; thus the latter technique was used for TSHZ3. OCT-embedded frozen tissue sections were fixed in pre-cooled acetone for 15 min, then washed twice in PBS. Primary antibodies were detected using appropriate Biotin-conjugated

secondary antibodies: 1:500, goat anti-guinea pig IgG (Abcam ab6970**)** and 1;200, goat polyclonal anti-rabbit IgG (Abcam ab6720) and a peroxidase-based system, generating a brown colour followed by haematoxylin counterstain (46). Negative controls omitted primary antibodies and these experiments showed no significant signal (data not shown).

Quantitation of glomeruli

The number of glomeruli was determined using kidney images acquire from multiple mid-sagittal longitudinal sections (12µm; *Tshz3*$^{+/lacZ}$, n=58; WT, n=52) of whole P60 adult kidneys (*Tshz3*$^{+/lacZ}$, n=4; WT, n=4) stained by hematoxylin/eosin. We used ImageJ(47) to measure the renal cortex area into which the number of glomeruli was counted. The results are reported as the number of glomeruli per area (glomeruli/cm^2).

Transmission electronic microscopy and quantification

Kidneys were perfused as described above, rapidly dissected and postfixed in 2% PFA, 2.5% glutaraldehyde in cacodylate buffer (pH 7.2) overnight at 4 °C. The kidneys were put in 1% OsO_4 solution in cacodylate buffer for 1 h on ice, then dehydrated on ice and embedded in resin (EPON 912). Sample were polymerized 48 h at 60 °C. Ultrathin sections (80-nm) performed on Leica UCT were poststained with 2% uranyl acetate, followed by Reynolds' lead citrate. Section were examined with a high-resolution transmission electron microscope (Tecnai G2 (FEI), Netherland) at 200 kV and images were acquired with a Veleta camera (Olympus). EM images were opened and analyzed with ImageJ software (48); the straight-line tool was used to measure GBM thickness and endothelial cell fenestration on randomly selected electron micrographs. The same approach was used for morphometric analysis of foot process width, as described previously (49, 50).

Blood samples

Blood samples were collected from *Tshz3*$^{+/LacZ}$ (n= 11; 5 females and 6 males) and WT mice (n=11; 6 females and 5 males) at 60 days-of-age. The mean values for body weight of *Tshz3*$^{+/LacZ}$ and wild-type were 38.27± 7.8 (n=11) and 33.01 ± 4.9 (n=11). Mice were anaesthetized by an intraperitoneal injection of ketamine/xylazine (0.1 ml/10 g body weight) prior to manipulation. Anesthesia was maintained by using 1.7% to 2.5% isoflurane delivered in 600 ml/min oxygen and a closely fitting facemask. Blood was collected by cardiocentesis puncture in heparinize tubes with EDTA and also in tubes without anticoagulant, centrifuging at 4 ºC immediately after extraction. The total blood volume in 30-40 g mice is approximately 2 to 3 ml. The maximum volume that could be collected safely at a single survival time point was approximately 800-1000 µl. Blood tests were outsourced to Laboklin G.m.b.H. and performed using a Siemens' high-volume hematology analyzer (ADVIA 2120i) and a Roche' chemistry analyzer (Cobas 8000 c701).

Urine samples

Urine samples were collected from *Tshz3*$^{+/LacZ}$ (n= 7; 4 females and 3 males) and WT mice (n=7; 6 females and 1 males) at 60 days-of-age.

Animals were placed in a clean, dry, empty, and transparent individual cage. A non-absorbable plastic, fully sanitizable material was laid on the floor of the cage. During urine collection, water bottles were provided but no food was given to limit contamination with faeces or animal feed. The mouse was monitored all time and removed as soon as it urinated. The voided urine was aspirated with a Gilson Pipetman and transfert to a 1.5 mL sterile microcentrifuge tube (kept on ice). Collected urine was stored at -80C prior to analysis. Due to the small amount of urine collected, the procedure was repeated during three consecutive days to obtain 300ul of urine for each mouse.

Urinary Proteomics

Sample Preparation: Urine samples were collected and frozen at -80°C as described above. Immediately before preparation, mice urine samples were thawed on ice. 150 µl of urine was mixed with a similar volume of a solution containing 2 M urea, 10 mM NH_4OH, and 0.02% sodium dodecyl sulfate (SDS). To remove high molecular weight molecules, samples were ultrafiltrated (3,400 × g for 45 min at 4°C) using a Centrisart 20kDa cut-off centrifugal filter device (Satorius, Göttingen, Germany) until 200 µl of filtrate was obtained. Afterwards, the filtrate was desalted by a NAP5 gel filtration column (GE Healthcare BioSciences, Uppsala, Sweden) to eliminate electrolytes and urea, hence decreasing matrix effects. The samples were lyophilized in a Savant SpeedVac SVC100H connected to a Virtis 3L Sentry freeze dryer (Fischer Scientific, Illkirch, France), consequently stored at 4°C. Shortly before CE-MS analysis, the samples were resuspended in 10 µl high-performance liquid chromatography grade water (HPLC-H_2O).

CE-MS analysis and data processing: CE-MS experiments were conducted as previously reported (51). Briefly, a Beckman Coulter Proteome Lab PA800 capillary electrophoresis system (Fullerton, CA) online coupled to a micrOTOF II MS (Bruker Daltonic, Bremen, Germany) was used. The electro-ionization (ESI) sprayer (Agilent Technologies, Palo Alto, CA) was grounded, and the ion spray interface potential was established to –4.5 kV. Subsequently, data acquisition and MS acquisition methods were automatically measured through the CE by contact-close-relays. Spectra were accrued every 3 seconds, over a range of m/z 350 to 3000.

Mass spectral ion peaks signifying identical molecules at different charges were deconvoluted into singles masses using MosaiquesVisu (52). The subsequent peak lists categorized each peptide according to its molecular mass (kDa), CE-migration time (min) and signal intensity (amplitude). Due to the analytical variances of urine samples,

484 migration time and ion signal intensity (amplitude) were normalized using endogenous
485 "housekeeping" peptides, normally displaying a small difference between at least 90% of
486 all urine samples, as reported elsewhere (51). Lastly, all detected peptides were deposited,
487 matched and annotated in a Microsoft SQL database (51). Thus, further comparisons and
488 statistical analysis among both groups were performed.
489 *Sequencing of peptides:* Tandem mass spectrometry (MS/MS) analysis were conducted
490 to retrieve the sequence information of the peptides, as previously described (51). Briefly,
491 MS/MS experiments were performed on a Dionex Ultimate 3000 RSLC nanoflow system
492 (Dionex, Camberly, UK) coupled to an Orbitrap Velos MS instrument (Thermo Fisher
493 Scientific). Thereafter, all resulting data files were evaluated by the use of SEQUEST
494 (using Thermo Proteome Discoverer 1.2) without any enzyme specificity and searched
495 beside the Swiss-Prot *Mus Musculus* database, as previously described(53).
496 *Statistical analysis:* For the identification of potential significant different urinary
497 peptides, urine samples from both groups (wild type and *Tshz3*$^{+/lacZ}$) were compared. *P*-
498 values were calculated according to the Wilcoxon Rank-Sum test. For multiple testing
499 correction, the reported *p*-values were further adjusted via false discovery rate method
500 described by Benjamini and Hochberg (54). Only peptides with p-values less than 0.05
501 and detected in a frequency threshold of ≥70% in at least one of both groups were further
502 considered as statistically significant. Statistical analysis was performed using Prism 7.05
503 (GraphPad Software, USA) and results considered significant at $P < 0.05$.
504
505 **Data availability**
506 The data that support the findings of this study are available from the corresponding
507 author upon reasonable request. Raw data (FastQ files) from the sequencing experiment
508 (triplicates from wild-type and *Tshz3*$^{+/lacZ}$ adult kidney) and raw abundance
509 measurements for genes (read counts) for each sample are available from Gene

Expression Omnibus (GEO) under accession GSE182010, which should be quoted in any manuscript discussing the data.

Ethics Statement

The Experiments were ethically approved by the 1) "*Comité National de Réflexion Ethique sur l'Expérimentation Animale* 14" (ID numbers 57-07112012) and were in agreement with the European Communities Council Directive (2010/63/EU); 2) Registered Medical and Scientific Departments of the University of Manchester. Mice were maintained in the Biological Services Colony at The University of Manchester under UK Home Office Project Licence PPL 40/3446.

Acknowledgements

We appreciate feedback on the manuscript provided by Pierre L. Roubertoux. Microscopy was performed at the imaging platform of the IBDM, supported by the ANR through the "Investments for the Future" program (France-BioImaging, ANR-10-INSB-04-01). This work was supported by the European Union's Horizon 2020 research and innovation programme under the Marie Sklodowska-Curie grant agreement No 642937 (Scientific coordinator L.F), the French National Research Agency (ANR-17-CE16-0030-01 "TSHZ3inASD" project to L.F.), the Centre National de la Recherche Scientifique (CNRS), the Institut National pour la Recherche Médicale (INSERM) and Aix-Marseille University. We acknowledge grant support from the Medical Research Council project grant (MR/T016809/1) and Kids Kidney Research/Kidney Research UK project grant (2010). I.S-M. and P.M. acknowledge financial support from the European Union's Horizon 2020 research and innovation PhD programme under the Marie Sklodowska-Curie grant agreement No 642937.

Conflict of Interest Statement

The authors declare no conflicts of interest and no competing financial interests.

References

1 Schedl, A. (2007) Renal abnormalities and their developmental origin. *Nat Rev Genet*, **8**, 791-802.

2 Chang, C.P., McDill, B.W., Neilson, J.R., Joist, H.E., Epstein, J.A., Crabtree, G.R. and Chen, F. (2004) Calcineurin is required in urinary tract mesenchyme for the development of the pyeloureteral peristaltic machinery. *J Clin Invest*, **113**, 1051-1058.

3 Klein, J., Gonzalez, J., Miravete, M., Caubet, C., Chaaya, R., Decramer, S., Bandin, F., Bascands, J.L., Buffin-Meyer, B. and Schanstra, J.P. (2011) Congenital ureteropelvic junction obstruction: human disease and animal models. *International Journal of Experimental Pathology*, **92**, 168-192.

4 Caubit, X., Gubellini, P., Andrieux, J., Roubertoux, P.L., Metwaly, M., Jacq, B., Fatmi, A., Had-Aissouni, L., Kwan, K.Y., Salin, P. *et al.* (2016) TSHZ3 deletion causes an autism syndrome and defects in cortical projection neurons. *Nat Genet*, **48**, 1359-1369.

5 Caubit, X., Lye, C.M., Martin, E., Core, N., Long, D.A., Vola, C., Jenkins, D., Garratt, A.N., Skaer, H., Woolf, A.S. *et al.* (2008) Teashirt 3 is necessary for ureteral smooth muscle differentiation downstream of SHH and BMP4. *Development*, **135**, 3301-3310.

6 Martin, E., Caubit, X., Airik, R., Vola, C., Fatmi, A., Kispert, A. and Fasano, L. (2013) TSHZ3 and SOX9 regulate the timing of smooth muscle cell differentiation in the ureter by reducing myocardin activity. *PLoS One*, **8**, e63721.

7 Caubit, X., Thoby-Brisson, M., Voituron, N., Filippi, P., Bevengut, M., Faralli, H., Zanella, S., Fortin, G., Hilaire, G. and Fasano, L. (2010) Teashirt 3 regulates development of neurons involved in both respiratory rhythm and airflow control. *J Neurosci*, **30**, 9465-9476.

8 Karaiskos, N., Rahmatollahi, M., Boltengagen, A., Liu, H., Hoehne, M., Rinschen, M., Schermer, B., Benzing, T., Rajewsky, N., Kocks, C. *et al.* (2018) A Single-Cell Transcriptome Atlas of the Mouse Glomerulus. *Journal of the American Society of Nephrology : JASN*, **29**, 2060-2068.

9 Park, J., Shrestha, R., Qiu, C., Kondo, A., Huang, S., Werth, M., Li, M., Barasch, J. and Susztak, K. (2018) Single-cell transcriptomics of the mouse kidney reveals potential cellular targets of kidney disease. *Science*, **360**, 758-763.

10 Liu, J., Krautzberger, A.M., Sui, S.H., Hofmann, O.M., Chen, Y., Baetscher, M., Grgic, I., Kumar, S., Humphreys, B.D., Hide, W.A. *et al.* (2014) Cell-specific translational profiling in acute kidney injury. *The Journal of clinical investigation*, **124**, 1242-1254.

11 Mootha, V.K., Lindgren, C.M., Eriksson, K.F., Subramanian, A., Sihag, S., Lehar, J., Puigserver, P., Carlsson, E., Ridderstrale, M., Laurila, E. *et al.* (2003) PGC-1alpha-responsive genes involved in oxidative phosphorylation are coordinately downregulated in human diabetes. *Nature Genetics*, **34**, 267-273.

12 Subramanian, A., Tamayo, P., Mootha, V.K., Mukherjee, S., Ebert, B.L., Gillette, M.A., Paulovich, A., Pomeroy, S.L., Golub, T.R., Lander, E.S. *et al.* (2005) Gene set enrichment analysis: a knowledge-based approach for interpreting genome-wide expression profiles. *Proceedings of the National Academy of Sciences of the United States of America*, **102**, 15545-15550.

13 Chen, E.Y., Tan, C.M., Kou, Y., Duan, Q., Wang, Z., Meirelles, G.V., Clark, N.R. and Ma'ayan, A. (2013) Enrichr: interactive and collaborative HTML5 gene list enrichment analysis tool. *BMC Bioinformatics*, **14**, 128.

14 Rubtsova, K., Rubtsov, A.V., van Dyk, L.F., Kappler, J.W. and Marrack, P. (2013) T-box transcription factor T-bet, a key player in a unique type of B-cell activation essential for effective viral clearance. *Proc. Natl. Acad. Sci. U. S. A.*, **110**, E3216-3224.
15 Good, D.M., Zurbig, P., Argiles, A., Bauer, H.W., Behrens, G., Coon, J.J., Dakna, M., Decramer, S., Delles, C., Dominiczak, A.F. *et al.* (2010) Naturally occurring human urinary peptides for use in diagnosis of chronic kidney disease. *Mol Cell Proteomics*, **9**, 2424-2437.
16 Caubit, X., Gubellini, P., Andrieux, J., Roubertoux, P.L., Metwaly, M., Jacq, B., Fatmi, A., Had-Aissouni, L., Kwan, K.Y., Salin, P. *et al.* (2016) TSHZ3 deletion causes an autism syndrome and defects in cortical projection neurons. *Nature Genetics*, **48**, 1359-1369.
17 Savige, J., Rana, K., Tonna, S., Buzza, M., Dagher, H. and Wang, Y.Y. (2003) Thin basement membrane nephropathy. *Kidney Int*, **64**, 1169-1178.
18 Dimke, H., Maezawa, Y. and Quaggin, S.E. (2015) Crosstalk in glomerular injury and repair. *Curr Opin Nephrol Hypertens*, **24**, 231-238.
19 Magalhaes, P., Pejchinovski, M., Markoska, K., Banasik, M., Klinger, M., Svec-Billa, D., Rychlik, I., Rroji, M., Restivo, A., Capasso, G. *et al.* (2017) Association of kidney fibrosis with urinary peptides: a path towards non-invasive liquid biopsies? *Sci Rep*, **7**, 16915.
20 Wei, R., Gao, B., Shih, F., Ranger, A., Dearth, A., Mischak, H., Siwy, J., Wisniacki, N., Petri, M. and Burkly, L.C. (2017) Alterations in urinary collagen peptides in lupus nephritis subjects correlate with renal dysfunction and renal histopathology. *Nephrol Dial Transplant*, **32**, 1468-1477.
21 Klein, J., Ramirez-Torres, A., Ericsson, A., Huang, Y., Breuil, B., Siwy, J., Mischak, H., Peng, X.R., Bascands, J.L. and Schanstra, J.P. (2016) Urinary peptidomics provides a noninvasive humanized readout of diabetic nephropathy in mice. *Kidney Int*, **90**, 1045-1055.
22 Mudge, J.M., Armstrong, S.D., McLaren, K., Beynon, R.J., Hurst, J.L., Nicholson, C., Robertson, D.H., Wilming, L.G. and Harrow, J.L. (2008) Dynamic instability of the major urinary protein gene family revealed by genomic and phenotypic comparisons between C57 and 129 strain mice. *Genome Biol*, **9**, R91.
23 Thoss, M., Luzynski, K.C., Enk, V.M., Razzazi-Fazeli, E., Kwak, J., Ortner, I. and Penn, D.J. (2019) Regulation of volatile and non-volatile pheromone attractants depends upon male social status. *Sci Rep*, **9**, 489.
24 Gallagher, J.C. and Seligson, D. (1962) Significance of abnormally low blood urea levels. *N Engl J Med*, **266**, 492-495.
25 Lum, G. and Leal-Khouri, S. (1989) Significance of low serum urea nitrogen concentrations. *Clin Chem*, **35**, 639-640.
26 de Baaij, J.H., Hoenderop, J.G. and Bindels, R.J. (2012) Regulation of magnesium balance: lessons learned from human genetic disease. *Clin Kidney J*, **5**, i15-i24.
27 Liu, S. and Quarles, L.D. (2007) How fibroblast growth factor 23 works. *J Am Soc Nephrol*, **18**, 1637-1647.
28 Lederer, E. (2014) Regulation of serum phosphate. *J Physiol*, **592**, 3985-3995.
29 Traslavina, R.P., King, E.J., Loar, A.S., Riedel, E.R., Garvey, M.S., Ricart-Arbona, R., Wolf, F.R. and Couto, S.S. (2010) Euthanasia by CO(2) inhalation affects potassium levels in mice. *J Am Assoc Lab Anim Sci*, **49**, 316-322.

30 Kim, W.Y., Lee, H.W., Han, K.H., Nam, S.A., Choi, A., Kim, Y.K. and Kim, J. (2016) Descending thin limb of the intermediate loop expresses both aquaporin 1 and urea transporter A2 in the mouse kidney. *Histochem Cell Biol*, **146**, 1-12.
31 Pannabecker, T.L. (2012) Structure and function of the thin limbs of the loop of Henle. *Compr Physiol*, **2**, 2063-2086.
32 van der Wijst, J., Belge, H., Bindels, R.J.M. and Devuyst, O. (2019) Learning Physiology From Inherited Kidney Disorders. *Physiol Rev*, **99**, 1575-1653.
33 Clothier, J. and Absoud, M. (2020) Autism spectrum disorder and kidney disease. *Pediatr Nephrol*, in press.
34 Meyer, E., Carss, K.J., Rankin, J., Nichols, J.M., Grozeva, D., Joseph, A.P., Mencacci, N.E., Papandreou, A., Ng, J., Barral, S. *et al.* (2017) Mutations in the histone methyltransferase gene KMT2B cause complex early-onset dystonia. *Nat Genet*, **49**, 223-237.
35 Scarfe, L., Rak-Raszewska, A., Geraci, S., Darssan, D., Sharkey, J., Huang, J., Burton, N.C., Mason, D., Ranjzad, P., Kenny, S. *et al.* (2015) Measures of kidney function by minimally invasive techniques correlate with histological glomerular damage in SCID mice with adriamycin-induced nephropathy. *Sci Rep*, **5**, 13601.
36 Paroly, S.S., Wang, F., Spraggon, L., Merregaert, J., Batourina, E., Tycko, B., Schmidt-Ott, K.M., Grimmond, S., Little, M. and Mendelsohn, C. (2013) Stromal protein Ecm1 regulates ureteric bud patterning and branching. *PLoS One*, **8**, e84155.
37 Wu, L.L., Mao, S.S., Lin, X., Yang, R.W. and Zhu, Z.W. (2019) Evaluation of Whole Blood Trace Element Levels in Chinese Children with Autism Spectrum Disorder. *Biol Trace Elem Res*, **191**, 269-275.
38 Saldanha Tschinkel, P.F., Bjorklund, G., Conon, L.Z.Z., Chirumbolo, S. and Nascimento, V.A. (2018) Plasma concentrations of the trace elements copper, zinc and selenium in Brazilian children with autism spectrum disorder. *Biomed Pharmacother*, **106**, 605-609.
39 Strambi, M., Longini, M., Hayek, J., Berni, S., Macucci, F., Scalacci, E. and Vezzosi, P. (2006) Magnesium profile in autism. *Biol Trace Elem Res*, **109**, 97-104.
40 Guo, M., Li, L., Zhang, Q., Chen, L., Dai, Y., Liu, L., Feng, J., Cai, X., Cheng, Q., Chen, J. *et al.* (2020) Vitamin and mineral status of children with autism spectrum disorder in Hainan Province of China: associations with symptoms. *Nutr Neurosci*, **23**, 803-810.
41 Subramanian, A., Tamayo, P., Mootha, V.K., Mukherjee, S., Ebert, B.L., Gillette, M.A., Paulovich, A., Pomeroy, S.L., Golub, T.R., Lander, E.S. *et al.* (2005) Gene set enrichment analysis: a knowledge-based approach for interpreting genome-wide expression profiles. *Proc Natl Acad Sci U S A*, **102**, 15545-15550.
42 Mootha, V.K., Lindgren, C.M., Eriksson, K.F., Subramanian, A., Sihag, S., Lehar, J., Puigserver, P., Carlsson, E., Ridderstrale, M., Laurila, E. *et al.* (2003) PGC-1alpha-responsive genes involved in oxidative phosphorylation are coordinately downregulated in human diabetes. *Nat Genet*, **34**, 267-273.
43 Livak, K.J. and Schmittgen, T.D. (2001) Analysis of relative gene expression data using real-time quantitative PCR and the 2(-Delta Delta C(T)) Method. *Methods*, **25**, 402-408.
44 Relaix, F., Rocancourt, D., Mansouri, A. and Buckingham, M. (2004) Divergent functions of murine Pax3 and Pax7 in limb muscle development. *Genes Dev*, **18**, 1088-1105.
45 Yuan, H.T., Suri, C., Landon, D.N., Yancopoulos, G.D. and Woolf, A.S. (2000) Angiopoietin-2 is a site-specific factor in differentiation of mouse renal vasculature. *J Am Soc Nephrol*, **11**, 1055-1066.

46 Anders, C., Ashton, N., Ranjzad, P., Dilworth, M.R. and Woolf, A.S. (2013) Ex vivo modeling of chemical synergy in prenatal kidney cystogenesis. *PLoS One*, **8**, e57797.
47 Schneider, C.A., Rasband, W.S. and Eliceiri, K.W. (2012) NIH Image to ImageJ: 25 years of image analysis. *Nat Methods*, **9**, 671-675.
48 Schneider, C.A., Rasband, W.S. and Eliceiri, K.W. (2012) NIH Image to ImageJ: 25 years of image analysis. *Nat Methods*, **9**, 671-675.
49 van den Berg, J.G., van den Bergh Weerman, M.A., Assmann, K.J., Weening, J.J. and Florquin, S. (2004) Podocyte foot process effacement is not correlated with the level of proteinuria in human glomerulopathies. *Kidney Int*, **66**, 1901-1906.
50 Deegens, J.K., Dijkman, H.B., Borm, G.F., Steenbergen, E.J., van den Berg, J.G., Weening, J.J. and Wetzels, J.F. (2008) Podocyte foot process effacement as a diagnostic tool in focal segmental glomerulosclerosis. *Kidney Int*, **74**, 1568-1576.
51 von zur Muhlen, C., Schiffer, E., Sackmann, C., Zurbig, P., Neudorfer, I., Zirlik, A., Htun, N., Iphofer, A., Jansch, L., Mischak, H. *et al.* (2012) Urine proteome analysis reflects atherosclerotic disease in an ApoE-/- mouse model and allows the discovery of new candidate biomarkers in mouse and human atherosclerosis. *Molecular & cellular proteomics : MCP*, **11**, M111 013847.
52 Neuhoff, N., Kaiser, T., Wittke, S., Krebs, R., Pitt, A., Burchard, A., Sundmacher, A., Schlegelberger, B., Kolch, W. and Mischak, H. (2004) Mass spectrometry for the detection of differentially expressed proteins: a comparison of surface-enhanced laser desorption/ionization and capillary electrophoresis/mass spectrometry. *Rapid communications in mass spectrometry : RCM*, **18**, 149-156.
53 Nkuipou-Kenfack, E., Schanstra, J.P., Bajwa, S., Pejchinovski, M., Vinel, C., Dray, C., Valet, P., Bascands, J.L., Vlahou, A., Koeck, T. *et al.* (2017) The use of urinary proteomics in the assessment of suitability of mouse models for ageing. *PLoS One*, **12**, e0166875.
54 Benjamini, Y. and Hochberg, Y. (1995) Controlling the False Discovery Rate: A Practical and Powerful Approach to Multiple Testing. *Journal of the Royal Statistical Society. Series B (Methodological)*, **57**, 289-300.

Legends to Figures

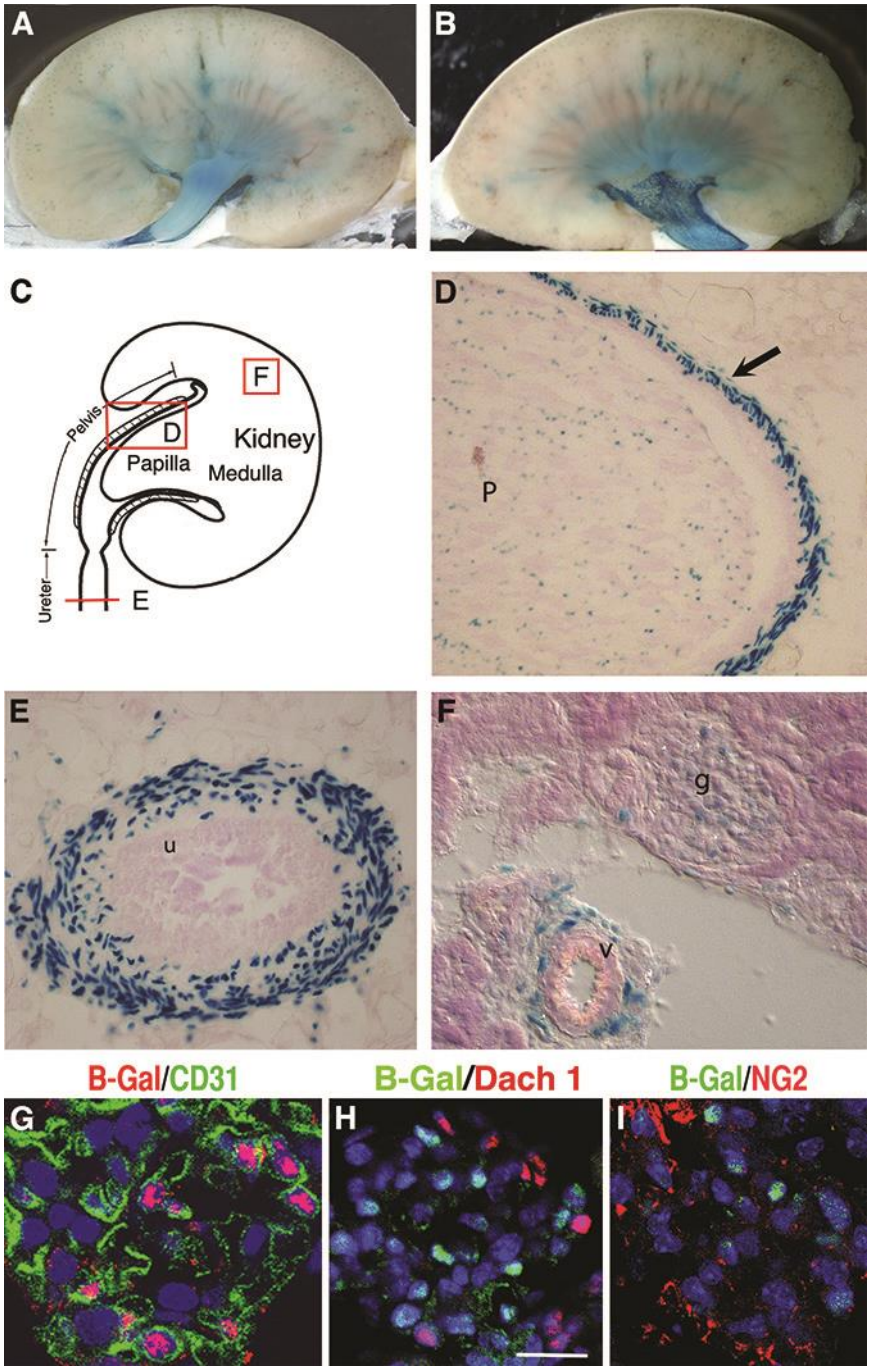

Figure 1. Distribution of Xgal-positive cells in *Tshz3*$^{+/lacZ}$ adult renal tract. (A, B) The two halves of the same adult kidney stained with X-Gal. (C) Cartoon showing the section sites and planes for D, E and F. (D-F) Xgal-Positive cells were found in papilla (p) and smooth muscle present in the pelvic region (arrow) (D), in the mesenchymal part of the ureter (E), in the glomeruli (g) and in close proximity to blood vessel (v) (F). (G-I) In glomeruli, TSHZ3 (ß-Gal) is detected in CD31+ glomerular endothelial cells (G) but not

in DACH1+ podocytes (H) or in NG2+ mesangial cells (I); scale bar, in G-I, 20 µm. B-Gal, Beta-Galactosidase; u: urothelium.

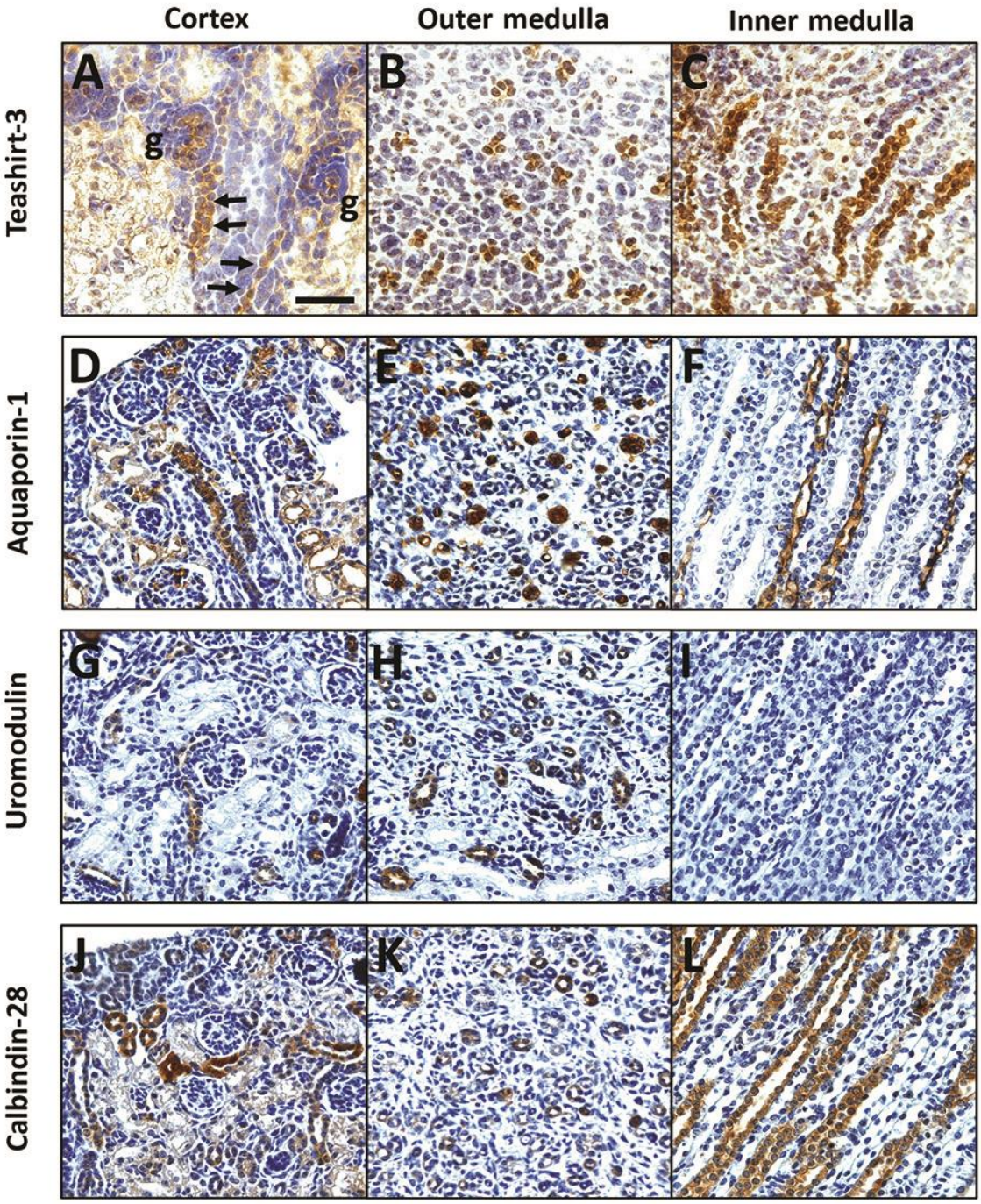

Figure 2. Immunohistochemistry for TSHZ3 and kidney segment markers. Immunohistochemistry (brown positive signal) of one week postnatal *Tshz3*$^{+/lacZ}$ mouse kidneys for: A-C. Teashirt-3 (TSHZ3); D-F. Aquaporin-1 (marker of proximal tubules and thin descending limb of loop of Henle; G-I. Uromodulin (marker of the thick

ascending limb of loop of Henle); and J-L. Calbindin-28 (marker of distal nephron tubules and collecting ducts). A-C are from frozen sections, and D-L are from paraffin-embedded sections; the latter processing tends to make the tissue appear more compact. All sections counterstained with haemotoxylin (blue nuclei). A, D, G and J show the cortex, with the outside of the organ uppermost; B, E, H and K are transverse sections through the outer medulla; and C, F, I and L are longitudinal sections through the inner medulla. In the cortex (A), TSHZ3 was immunodetected in nuclei within tufts of maturing glomeruli (g) and in nuclei of thin tubule-like structures (arrowed). Subsets of tubule-like profiles also immunostained for TSHZ3 in the outer medulla (B) and the inner medulla (C). Comparison with immunostaining patterns for aquaporin-1, uromodulin and calbindin-28, suggest that thin descending limbs of loops of Henle express TSHZ3 because patterns for this protein and aquaporin-1 are similar in the thin tubules within the inner medulla. In this location, calbinin-28 positive collecting ducts are wider diameter and uromodulin is not detected. The TSHZ3 positive tubules in the cortex and outer medulla may also include the pars recta, or straight section, of the aquaporin-1 positive proximal tubule. Bars are 50 µm.

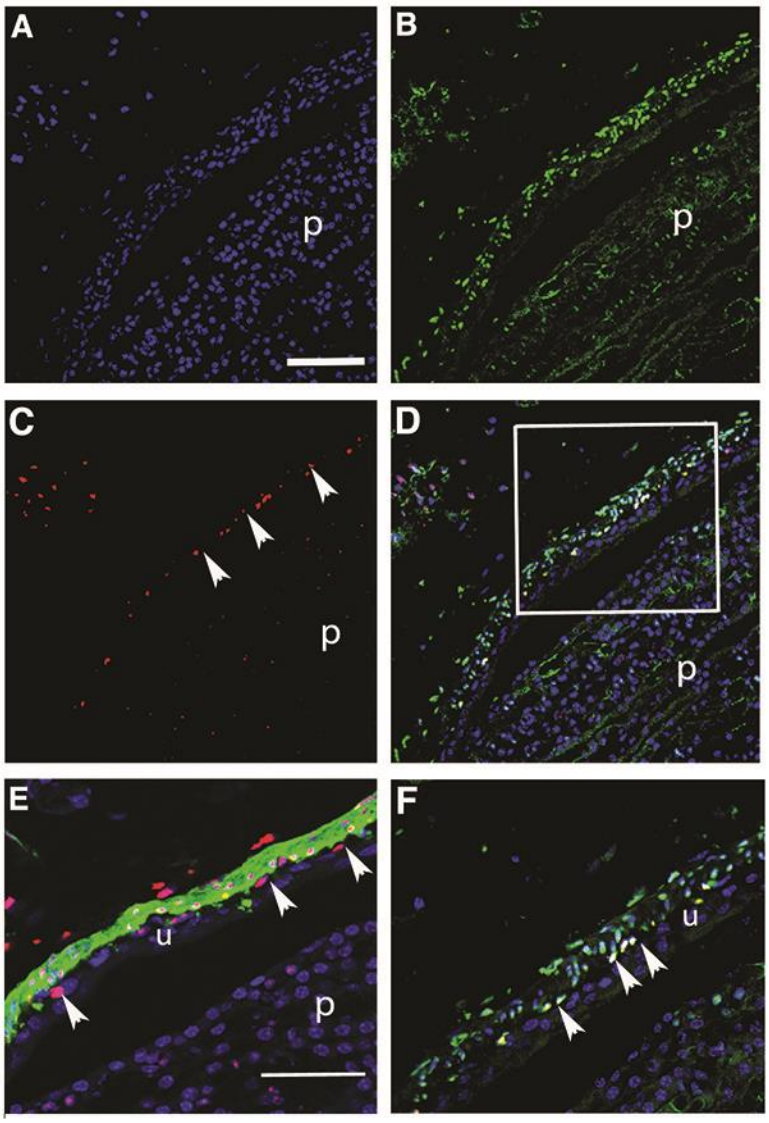

Figure 3. Characterization of β-galactosidase-positive cells in the pelvic region of *Tshz3*$^{+/lacZ}$ adult kidney. (A-D) Comparative expression of ß-galactosidase (green) and Dachshund 1 (red) in the pelvic region. (F) Close up of the region boxed in D. Merge image (D, F) shows that a subset of βgal+ cells expresses DACH1 (arrowheads in C and F). These cells represent a cell layer in a sub urothelial position. (E) Double immunostaining for βgalactosidase (red) and smooth muscle actin (green) indicates that βgal expression is found in SMA expressing cells. Some βgal+ cells adjacent to the urothelium do not express SMA (arrowheads in E). P: papilla, u: urothelium. Scale bars, in A, 100µm; in E, 50µm.

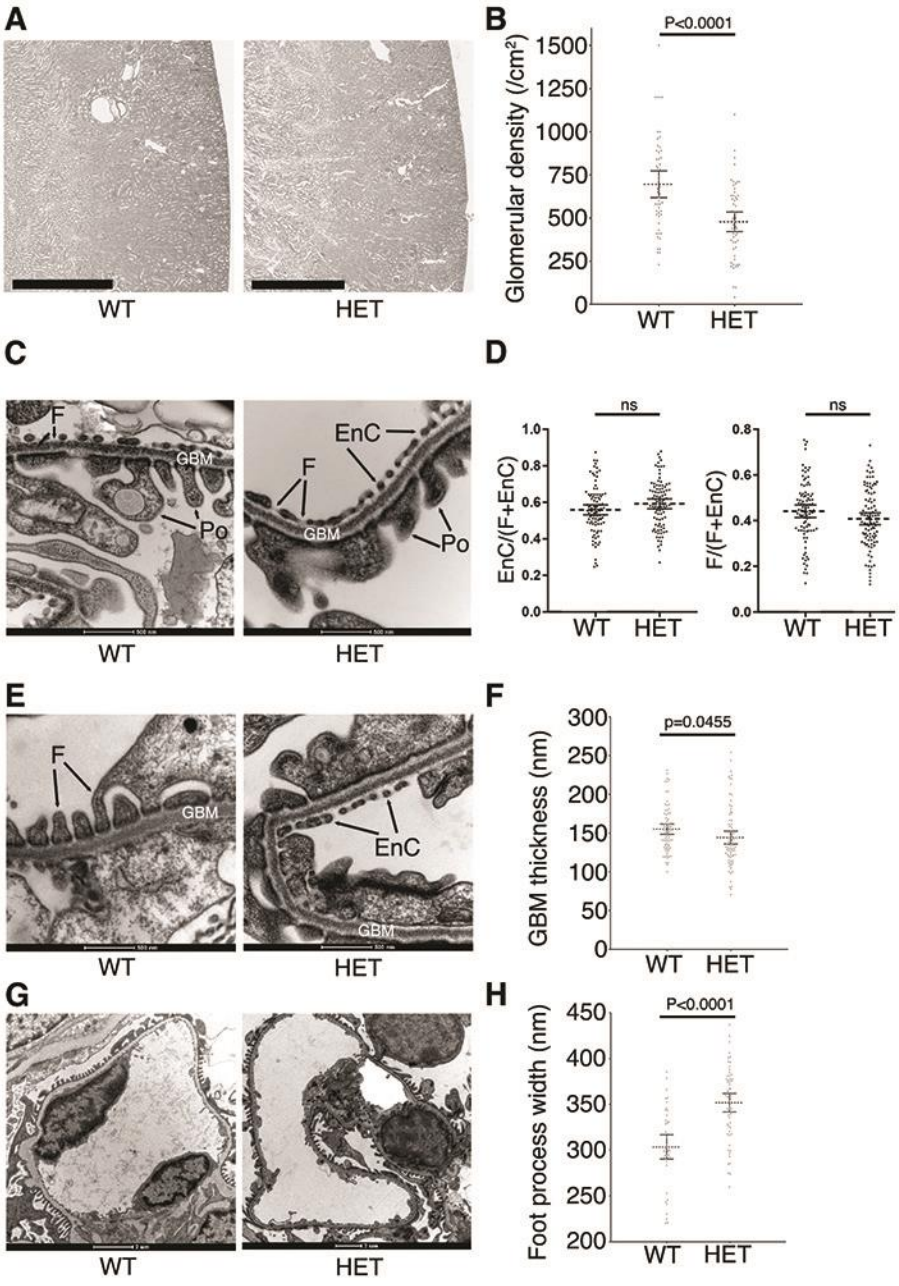

Figure 4: Reduced glomerular density, glomerular basement membrane thinning and larger foot process width in heterozygous *Tshz3*$^{lacZ/+}$ mice. (A) Representative images of haematoxylin and eosin-stained sections of WT and *Tshz3*$^{+/lacZ}$ adult kidneys at post-natal day 60. Scale bar 1mm. (B) The graph shows the significant (P<0.0001) reduction of the glomerular density in heterozygous *Tshz3*$^{lacZ/+}$ (471 ± 0.29 /cm^2, 48 sections from 3 kidneys) compare to wild-type kidney (695 ± 0.38 /cm^2, 41 sections from 3 kidneys). (C, E, G) Representative TEM images of wild type and *Tshz3*$^{+/lacZ}$ adult kidneys. (D, F, H) TEM morphometric analysis. (C) TEM: No abnormalities in endothelial cell fenestration are observe in *Tshz3*$^{+/lacZ}$ mice. Scale bar, 500nm. (D)

Morphometric analysis of the fenestration reveals no significant difference between WT and *Tshz3*$^{+/lacZ}$ mice. (E) TEM: *Tshz3*$^{+/lacZ}$ kidney shows a reduction of the thickness of the GBM in *Tshz3*$^{lacZ/+}$ compared to WT. Scale bar, 500nm. (F) Morphometric analysis reveals a significant reduction (P<0.0455) of the thickness of the GBM in *Tshz3*$^{lacZ/+}$ (144.2 ± 4.2 nm, 84 sections from 3 kidneys) compare to wild-type (155.1 ± 3.32 nm, 78 sections from 3 kidneys). (G) TEM: illustrating foot processes in *Tshz3*$^{lacZ/+}$ and WT mice. Scale bar, 2µm. (H) Foot process width in *Tshz3*$^{lacZ/+}$ (351.7 ± 5.03 nm, 61 sections from 9 kidneys) is significantly larger (P<0.0001) compared to WT (303.4 ± 6.57 nm, 42 sections from 7 kidneys) mice. Data are shown as mean and its 95% CI. EnC, endothelial cell cytoplasm; F, endothelial fenestration; GBM, glomerular basement membrane; HET, hererozygous; Po, podocyte foot process; SD, standard deviation; WT, wild type.

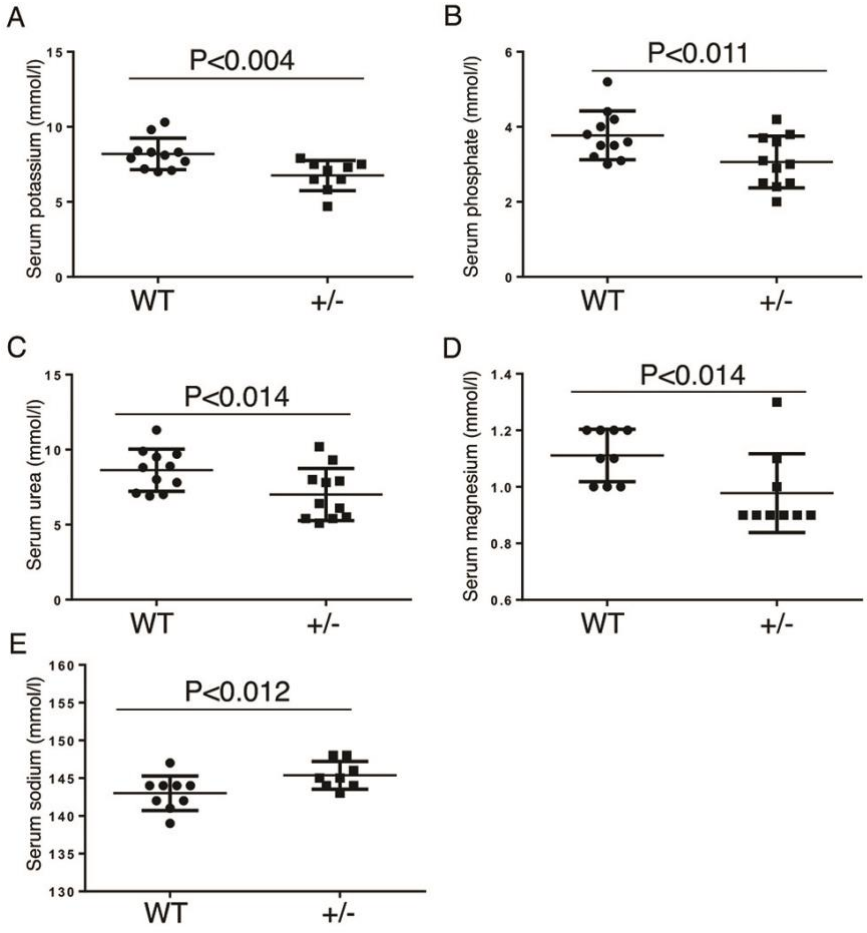

Figure 5. **Differences in serum biochemical parameters between control and *Tshz3*$^{lacZ/+}$ mice**. Plasma concentration of potassium (A), phosphates (B), urea (C), magnesium (D) and sodium (E). Data are represented as means ± SEM. Statistically significant difference from control at *p<0.02; **p<0.004. WT, wild type; +/-, *Tshz3*$^{+/lacZ}$

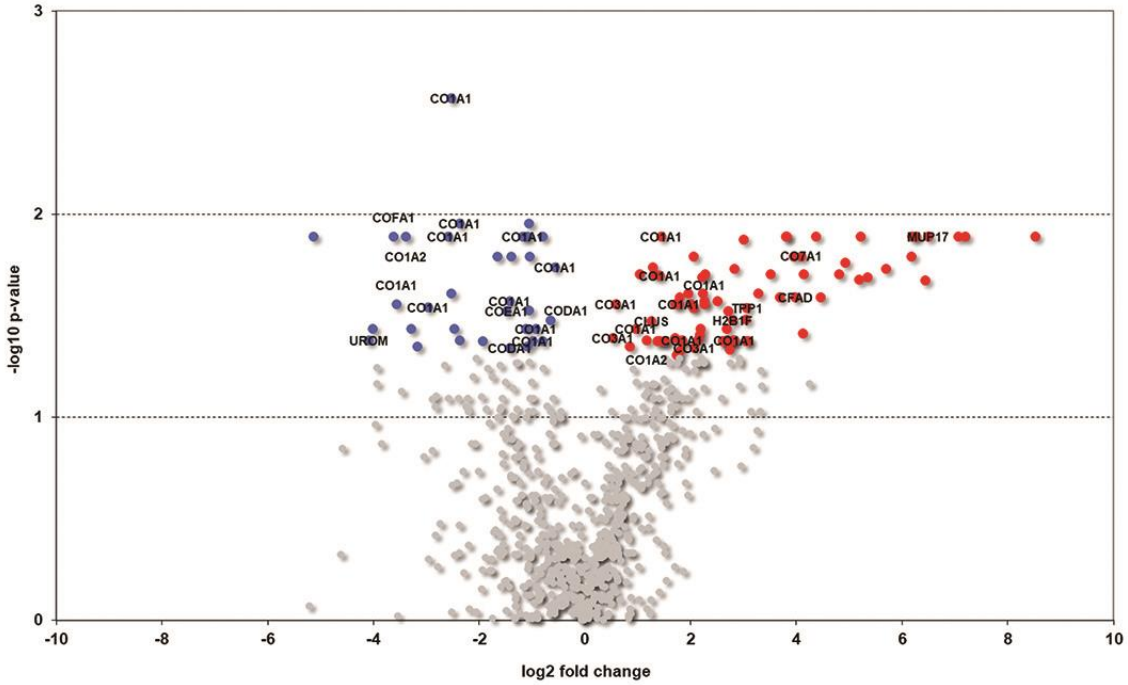

Figure 6. Urinary peptides displaying differential abundance in *Tshz3*$^{+/LacZ}$ mice. The volcano plot of quantified proteins revealed that 115 peptides (red and blue dots) show a significant change (p-value <0.05) in *Tshz3*$^{+/lacZ}$ compared to control mice. However, for 33 of these peptides we were able to find a sequence (labeled ones; see **Table 1i**). The grey dots are peptides that have not a significant change (p-value >0.05).

Supplementary Figures

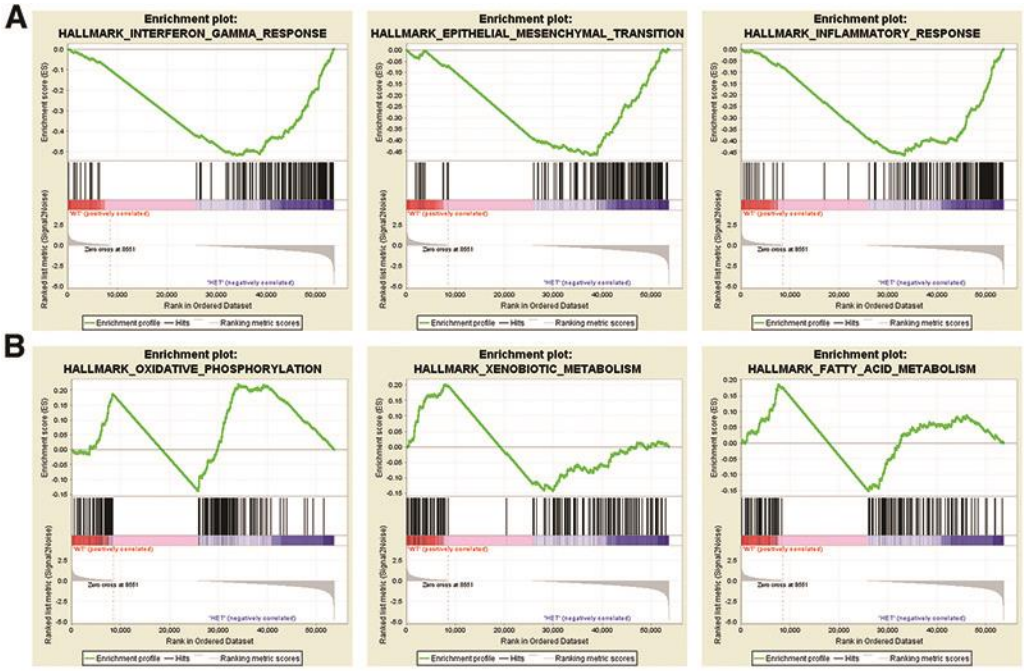

Supplementary figure 1: Enrichment plots from gene enrichment analysis (GSEA). GSEA results showing positive **(A)** and negative (**B**) enrichment in the kidneys of *Tshz3*$^{+/lacZ}$ adult mice for gene sets related to "interferon gamma response", "epithelial to mesenchymal transition", "inflammatory response" (**A**) and to "Oxydative Phosphorylation", "Xenobiotic Metabolism" and Fatty Acid Metabolism (**B**).

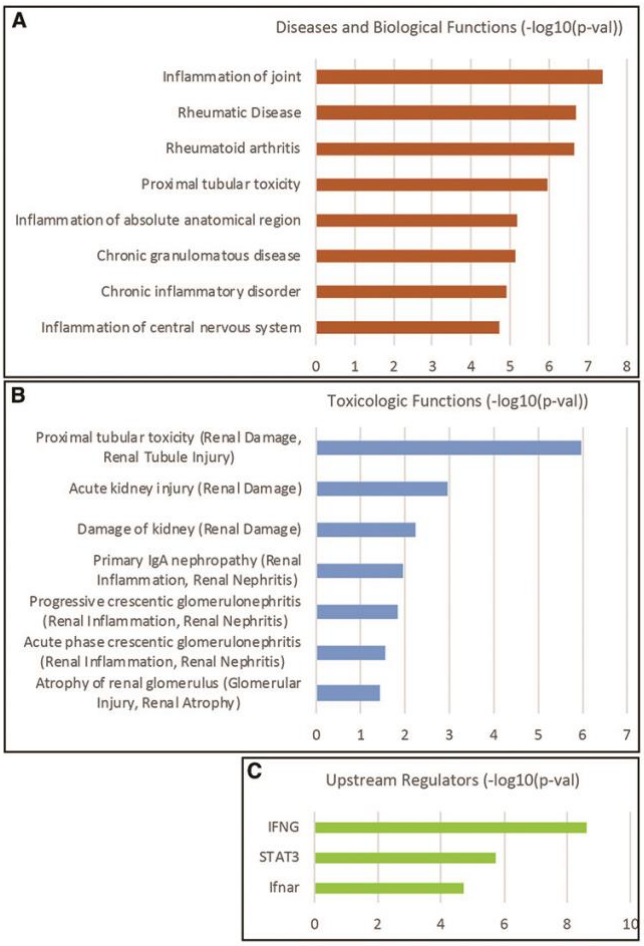

Supplementary Figure 2: Functional characterization of differentially expressed genes (DEGs) in *Tshz3*$^{+/lacZ}$ adult kidneys, using Ingenuity Pathway Analysis (IPA). (A) Significant enrichments observed in the Diseases and Biological Functions annotations. (B) Relevant toxicity phenotypes and clinical pathology endpoints associated with the DEGs. (C) Major upstream regulators of the DEGs. Minus Log of the p-values calculated from Fisher's exact test are shown on the x-axis.

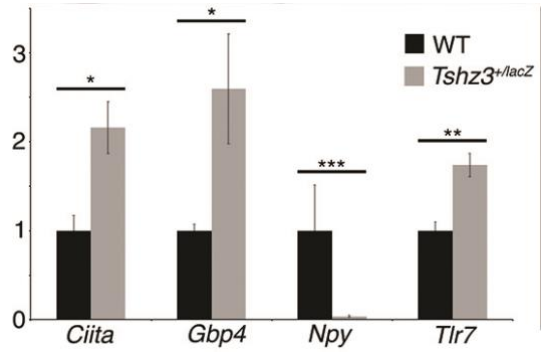

Supplementary figure 3: Quantitative real-time PCR validation of four differentially expressed genes in *Tshz3*$^{+/lacZ}$ kidney as identified by RNAseq. Bar graph showing significant variation in mRNA levels as determined by qRT–PCR in *Tshz3*$^{+/lacZ}$ versus WT mice for *Ciita*, *Gbp4*, *Npy* and *Tlr7*. Data are shown as means ± s.e.m. Unpaired two-tailed t test. *, P <0.03; **, P <0.006; ***, P <0.002.

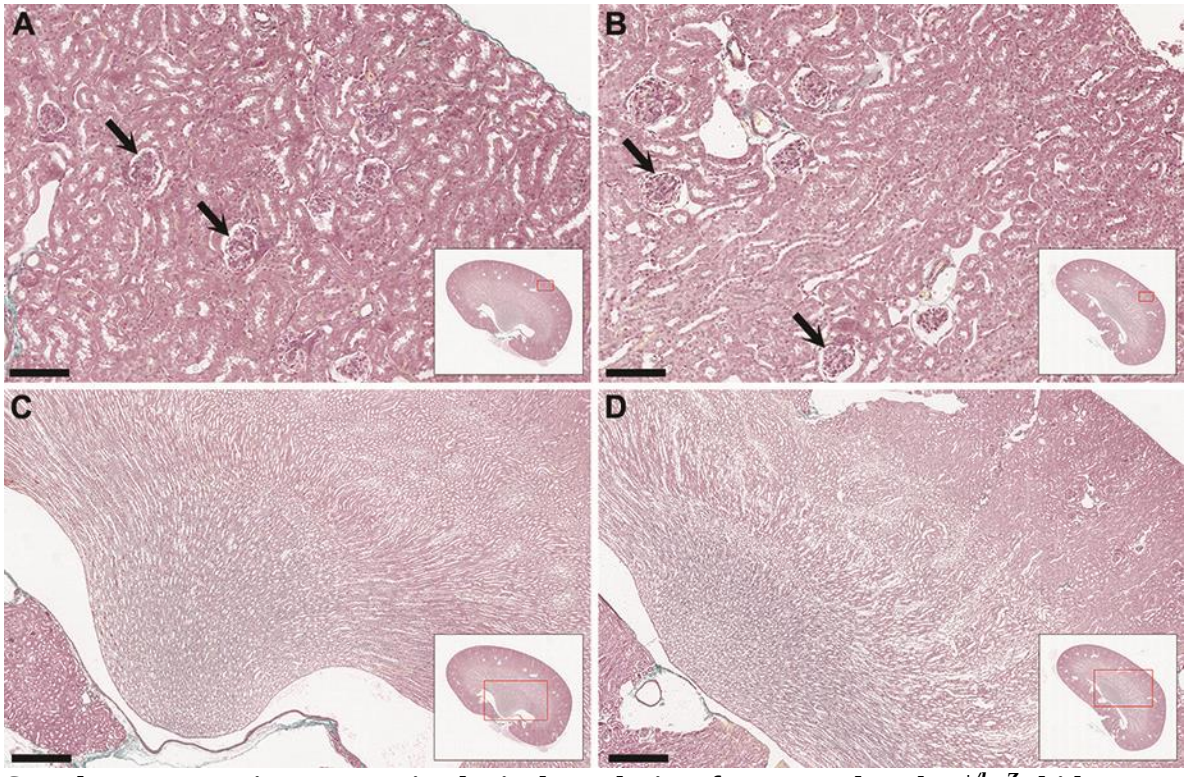

Supplementary Figure 4. Histological analysis of WT and *Tshz3*$^{+/lacZ}$ kidney. Representative images of haematoxylin and eosin-stained sections of WT (A, C) and *Tshz3*$^{+/lacZ}$ (B, D) adult kidneys at post-natal day 60. Sections of the cortical region (A, B) and the papilla (C, D). Arrows indicate glomeruli. In the box showing the whole section, the red rectangle indicates which part of the section is shown as A, B, C or D. Scale bars, in A and B, 125µm; in C and D, 500µm.

841

Table 1a. Blood serum biochemical measurements for control and *Tshz3*$^{+/lacZ}$ mice.

Parameters (mmol/l)	Control (n=11)	Tshz3+/lacZ (n=11)	p-Value (t-test)
Potassium	8.31 ± 1.05	6.83 ± 0.97	P<0.004
Phosphates	3.77 ± 0.65	3.06 ± 0.61	P<0.011
Magnesium	1.11 ± 0.09	0.98 ± 0.074	P<0.014
Urea	8.6 ± 1.4	7.01 ± 1.8	P<0.014
Sodium	143 ± 2.1	145.36 ± 1.85	P<0.012

Blood serum biochemical measurements for control and *Tshz3*$^{+/lacZ}$ mice.

842
843

844

Table 1b. Significantly differentially expressed genes (DEGs) between WT and HET. FDR cutoff chosen was FDR <=0.01

Ensembl ID	Gene symbol	Gene Name	baseMean	log2 Fold Change	lfcSE	stat	pvalue	padj
ENSMUSG00000054676	1600014C10Rik	RIKEN cDNA 1600014C10 gene(1600014C10Rik)	7360,92	-0,63	0,14	-4,41	1,0E-05	6,1E-03
ENSMUSG00000086474	9130204K15Rik	RIKEN cDNA 9130204K15 gene	181,94	-0,78	0,21	-3,68	2,3E-04	6,9E-02
ENSMUSG00000004668	Abca13	ATP-binding cassette, sub-family A (ABC1), member 13	5366,75	0,63	0,18	3,52	4,4E-04	9,6E-02
ENSMUSG00000031659	Adcy7	Adenylate cyclase 7	474,95	0,73	0,20	3,62	2,9E-04	7,7E-02
ENSMUSG00000004730	Adgre1	Adhesion G protein-coupled receptor E1	387,86	0,69	0,20	3,49	4,8E-04	9,6E-02
ENSMUSG00000060470	Adgrg3	Adhesion G protein-coupled receptor G3	347,56	0,65	0,19	3,53	4,2E-04	9,6E-02
ENSMUSG00000085180	Ai838599	Expressed sequence AI838599	473,16	0,71	0,17	4,06	4,8E-05	2,2E-02
ENSMUSG00000033715	Akr1c14	aldo-keto reductase family 1, member C14(Akr1c14)	30143,69	-0,68	0,19	-3,53	4,2E-04	9,6E-02
ENSMUSG00000028356	Ambp	Alpha 1 microglobulin/bikunin precursor	105,82	0,89	0,22	4,08	4,4E-05	2,1E-02

ENSMUSG00000020609	Apob	Apolipoprotein B	6556,79	-0,58	0,17	-3,47	5,1E-04	9,97E-02
ENSMUSG00000040694	Apobec2	apolipoprotein B mRNA editing enzyme, catalytic polypeptide 2	175,14	1,27	0,21	5,94	2,8E-09	1,1E-05
ENSMUSG00000020604	Arsg	Arylsulfatase G	2625,23	-0,77	0,17	-4,59	4,5E-06	3,2E-03
ENSMUSG00000038704	Aspdh	aspartate dehydrogenase domain containing(Aspdh)	5008,26	-0,59	0,17	-3,51	4,4E-04	9,6E-02
ENSMUSG00000017929	B4galt5	UDP-Gal:betaGlcNAc beta 1,4-galactosyltransferase, polypeptide 5(B4galt5)	18312,69	-0,65	0,18	-3,62	2,9E-04	7,7E-02
ENSMUSG00000090486	BC035947	CDNA sequence BC035947	4151,57	-0,60	0,17	-3,48	5,0E-04	9,96E-02
ENSMUSG00000030268	Bcat1	branched chain aminotransferase 1	6109,75	-0,92	0,14	-6,51	7,7E-11	3,6E-07
ENSMUSG00000058914	C1qtnf3	C1q and tumor necrosis factor related protein 3(C1qtnf3)	9805,38	-0,72	0,20	-3,59	3,3E-04	8,3E-02
ENSMUSG00000022416	Cacna1i	calcium channel, voltage-dependent, alpha 1I subunit	126,26	0,91	0,21	4,24	2,2E-05	1,1E-02
ENSMUSG00000038128	Camk4	Calcium/calmodulin-dependent protein kinase IV	274,72	0,84	0,21	4,05	5,2E-05	2,2E-02

ENSMUSG00000024610	Cd74	CD74 antigen (invariant polypeptide of major histocompatibility complex, class II antigen-associated)(Cd74)	12439,99	0,62	0,18	3,47	5,2E-04	9,97E-02
ENSMUSG00000022504	Ciita	class II transactivator	431,87	1,10	0,19	5,86	4,6E-09	1,4E-05
ENSMUSG00000056025	Clca3a1	Chloride channel accessory 3A1	875,04	0,74	0,16	4,56	5,2E-06	3,6E-03
ENSMUSG00000040663	Clcf1	Cardiotrophin-like cytokine factor 1	246,91	0,74	0,20	3,65	2,6E-04	7,2E-02
ENSMUSG00000024330	Col11a2	Collagen, type XI, alpha 2	191,72	1,00	0,21	4,83	1,4E-06	1,4E-03
ENSMUSG00000030905	Crym	Crystallin, mu	2030,99	-0,87	0,20	-4,42	9,7E-06	6,1E-03
ENSMUSG00000038642	Ctss	Cathepsin S [Source:MGI Symbol;Acc:MGI:107341]	1091,27	0,74	0,16	4,73	2,3E-06	1,9E-03
ENSMUSG00000027014	Cwc22	CWC22 spliceosome-associated protein(Cwc22)	3557,88	1,18	0,16	7,26	3,8E-13	2,4E-09
ENSMUSG00000015340	Cybb	Cytochrome b-245, beta polypeptide	747,51	0,62	0,17	3,67	2,4E-04	6,9E-02
ENSMUSG00000074254	Cyp2a4	cytochrome P450, family 2, subfamily a, polypeptide 4(Cyp2a4)	9870,25	-0,53	0,14	-3,85	1,2E-04	4,2E-02
ENSMUSG00000108332	D530033B14Rik	RIKEN cDNA D530033B14 gen	751,19	-0,83	0,18	-4,66	3,1E-06	2,4E-03
ENSMUSG00000031294	D630029K05Rik	RIKEN cDNA D630029K05 gene(D630029K05Rik)	7305,09	-0,65	0,17	-3,75	1,8E-04	5,8E-02

ENSMUSG00000025279	Dnase1l3	Deoxyribonuclease 1-like 3	124,40	0,77	0,22	3,51	4,4E-04	9,6E-02
ENSMUSG00000040658	Dnph1	2,-deoxynucleoside 5,-phosphate N-hydrolase 1	926,16	-0,72	0,19	-3,71	2,1E-04	6,4E-02
ENSMUSG00000020143	Dock2	Dedicator of cyto-kinesis 2	420,46	0,84	0,20	4,25	2,1E-05	1,1E-02
ENSMUSG00000025153	Fasn	fatty acid synthase(Fasn)	17210,76	0,94	0,16	5,83	5,6E-09	1,5E-05
ENSMUSG00000003420	Fcgrt	Fc receptor, IgG, alpha chain transporter(Fcgrt)	14127,59	-0,74	0,14	-5,21	1,8E-07	3,8E-04
ENSMUSG00000078650	G6pc	glucose-6-phosphatase, catalytic(G6pc)	36170,90	-0,64	0,18	-3,51	4,6E-04	9,6E-02
ENSMUSG00000033676	Gabrb3	Gamma-aminobutyric acid (GABA) A receptor, subunit beta 3	6443,23	-0,75	0,15	-5,09	3,5E-07	5,5E-04
ENSMUSG00000040264	Gbp2b	Guanylate binding protein 2b	129,28	0,94	0,22	4,28	1,9E-05	9,6E-03
ENSMUSG00000079363	Gbp4	guanylate binding protein 4	1227,60	0,93	0,18	5,26	1,4E-07	3,3E-04
ENSMUSG00000046352	Gjb2	gap junction protein, beta 2(Gjb2)	10013,45	-0,50	0,14	-3,58	3,4E-04	8,4E-02
ENSMUSG00000066407	Gm10263	Predicted gene 10263	1387,86	-0,64	0,17	-3,88	1,0E-04	4,1E-02

ENSMUSG00000087353	Gm13727	Predicted gene 13727	121,13	1,13	0,22	5,15	2,7E-07	5,0E-04
ENSMUSG00000093006	Gm24157	Predicted gene, 24157	284,34	1,01	0,20	5,04	4,6E-07	6,2E-04
ENSMUSG00000098747	Gm27216	predicted gene 27216(Gm27216)	590,10	-0,88	0,21	-4,13	3,6E-05	1,7E-02
ENSMUSG00000110631	Gm42047	Predicted gene, 42047	281,02	0,69	0,19	3,62	3,0E-04	7,7E-02
ENSMUSG00000104737	Gm42937	Predicted gene 42937	180,85	0,84	0,22	3,86	1,1E-04	4,1E-02
ENSMUSG00000115154	Gm49067	Predicted gene, 49067	315,01	-0,67	0,19	-3,52	4,3E-04	9,6E-02
ENSMUSG00000111942	Gm5182	Predicted gene 5182	831,08	0,77	0,20	3,92	8,8E-05	3,6E-02
ENSMUSG00000072324	Gm8420	predicted gene 8420	98,70	2,07	0,22	9,36	7,8E-21	8,1E-17
ENSMUSG00000025534	Gusb	glucuronidase, beta(Gusb)	10329,15	-0,96	0,19	-5,07	3,9E-07	5,6E-04
ENSMUSG00000036594	H2-Aa	histocompatibility 2, class II antigen A, alpha(H2-Aa)	5036,52	0,49	0,14	3,55	3,8E-04	9,1E-02
ENSMUSG00000073421	H2-Ab1	histocompatibility 2, class II antigen A, beta 1(H2-Ab1)	4559,45	0,69	0,19	3,74	1,8E-04	5,9E-02
ENSMUSG00000037649	H2-DMa	Histocompatibility 2, class II, locus DMa [Source:MGI Symbol;Acc:MGI:95921]	615,87	0,76	0,20	3,73	1,9E-04	6,0E-02

ENSMUSG00000067235	H2-Q10	Histocompatibility 2, Q region locus 10	395,64	0,77	0,22	3,51	4,5E-04	9,6E-02
ENSMUSG00000034551	Hdx	Highly divergent homeobox	63,83	0,79	0,22	3,61	3,1E-04	7,9E-02
ENSMUSG00000054072	Iigp1	Interferon inducible GTPase 1	977,29	0,85	0,18	4,79	1,6E-06	1,5E-03
ENSMUSG00000000157	Itgb2l	Integrin beta 2-like	154,29	0,79	0,21	3,73	1,9E-04	6,0E-02
ENSMUSG00000058740	Kcnt1	Potassium channel, subfamily T, member 1	1126,40	0,64	0,16	4,04	5,4E-05	2,2E-02
ENSMUSG00000063177	Klk1b27	Kallikrein 1-related peptidase b27	46,56	0,72	0,20	3,50	4,7E-04	9,6E-02
ENSMUSG00000028581	Laptm5	Lysosomal-associated protein transmembrane 5	978,54	0,61	0,17	3,56	3,7E-04	8,9E-02
ENSMUSG00000022587	Ly6e	lymphocyte antigen 6 complex, locus E(Ly6e)	16502,33	-0,47	0,13	-3,57	3,6E-04	8,9E-02
ENSMUSG00000069516	Lyz2	lysozyme 2(Lyz2)	2476,37	0,86	0,17	5,01	5,6E-07	6,9E-04
ENSMUSG00000012187	Mogat1	monoacylglycerol O-acyltransferase 1(Mogat1)	4309,18	-0,88	0,20	-4,41	1,0E-05	6,1E-03
ENSMUSG00000046805	Mpeg1	Macrophage expressed gene 1	1305,66	0,74	0,16	4,76	2,0E-06	1,7E-03
ENSMUSG00000022679	Mpv17l	Mpv17 transgene, kidney disease mutant-like(Mpv17l)	85348,94	-0,60	0,17	-3,54	4,0E-04	9,3E-02

ENSMUSG00000019992	Mtfr2	Mitochondrial fission regulator 2	47,96	0,79	0,22	3,65	2,6E-04	7,2E-02
ENSMUSG00000038670	Mybpc2	Myosin binding protein C, fast-type	151,73	0,76	0,22	3,47	5,1E-04	9,97E-02
ENSMUSG00000001056	Nhp2	NHP2 ribonucleoprotein(Nhp2)	3353,02	-0,66	0,19	-3,50	4,6E-04	9,6E-02
ENSMUSG00000074151	Nlrc5	NLR family, CARD domain containing 5	375,84	0,81	0,21	3,87	1,1E-04	4,1E-02
ENSMUSG00000029819	Npy	neuropeptide Y(Npy)	221,31	-1,99	0,21	-9,35	8,7E-21	8,1E-17
ENSMUSG00000032690	Oas2	2,-5, oligoadenylate synthetase 2	158,43	0,79	0,22	3,69	2,2E-04	6,8E-02
ENSMUSG00000021913	Ogdhl	Oxoglutarate dehydrogenase-like	276,39	0,86	0,21	4,04	5,3E-05	2,2E-02
ENSMUSG00000038910	Plcl2	Phospholipase C-like 2	782,25	-0,82	0,18	-4,63	3,7E-06	2,8E-03
ENSMUSG00000052160	Pld4	Phospholipase D family, member 4	403,71	0,79	0,18	4,41	1,0E-05	6,1E-03
ENSMUSG00000042251	Pm20d1	Peptidase M20 domain containing 1	9189,12	-0,67	0,18	-3,81	1,4E-04	4,8E-02
ENSMUSG00000030423	Pop4	Processing of precursor 4, ribonuclease P/MRP family	634,04	0,72	0,17	4,29	1,8E-05	9,6E-03
ENSMUSG00000020684	Rasl10b	RAS-like, family 10, member B	149,28	1,06	0,22	4,83	1,4E-06	1,4E-03

ENSMUSG00000021876	Rnase4	ribonuclease, RNase A family 4(Rnase4)	4455,76	-0,66	0,15	-4,38	1,2E-05	6,8E-03
ENSMUSG00000031609	Sap30	sin3 associated polypeptide(Sap30)	3295,63	-0,59	0,16	-3,67	2,4E-04	6,9E-02
ENSMUSG00000038224	Serpinf2	serine (or cysteine) peptidase inhibitor, clade F, member 2(Serpinf2)	21474,96	-0,78	0,20	-3,86	1,1E-04	4,1E-02
ENSMUSG00000035699	Slc51a	solute carrier family 51, alpha subunit(Slc51a)	6523,70	-0,65	0,17	-3,75	1,8E-04	5,8E-02
ENSMUSG00000025790	Slco3a1	Solute carrier organic anion transporter family, member 3a1	11292,58	-0,67	0,19	-3,50	4,7E-04	9,6E-02
ENSMUSG00000040693	Slco4c1	Solute carrier organic anion transporter family, member 4C1	324,30	0,76	0,20	3,86	1,1E-04	4,1E-02
ENSMUSG00000044349	Snhg11	Small nucleolar RNA host gene 11	2094,32	0,99	0,19	5,11	3,2E-07	5,5E-04
ENSMUSG00000096054	Syne1	Spectrin repeat containing, nuclear envelope 1	1889,03	0,59	0,17	3,52	4,3E-04	9,6E-02
ENSMUSG00000056296	Synpr	Synaptoporin	1611,78	-0,90	0,19	-4,66	3,1E-06	2,4E-03
ENSMUSG00000022218	Tgm1	transglutaminase 1, K polypeptide(Tgm1)	5200,82	-0,67	0,16	-4,31	1,7E-05	9,2E-03

ENSMUSG00000044583	Tlr7	Toll-like receptor 7	165,79	0,86	0,21	4,05	5,1E-05	2,2E-02
ENSMUSG00000040883	Tmem205	Transmembrane protein 205	4488,10	-0,59	0,16	-3,66	2,6E-04	7,2E-02
ENSMUSG00000048572	Tmem252	transmembrane protein 252(Tmem252)	6035,70	-0,70	0,20	-3,49	4,8E-04	9,6E-02
ENSMUSG00000010307	Tmem86a	transmembrane protein 86A(Tmem86a)	5856,74	-0,74	0,19	-3,84	1,2E-04	4,3E-02
ENSMUSG00000016942	Tmprss6	Transmembrane serine protease 6	518,88	0,74	0,20	3,63	2,8E-04	7,6E-02
ENSMUSG00000043621	Ubxn10	UBX domain protein 10	675,26	-0,80	0,21	-3,88	1,1E-04	4,1E-02
ENSMUSG00000031710	Ucp1	uncoupling protein 1 (mitochondrial, proton carrier)(Ucp1)	932,71	-0,94	0,21	-4,53	5,9E-06	3,9E-03
ENSMUSG00000027962	Vcam1	Vascular cell adhesion molecule 1	1251,88	0,77	0,16	4,81	1,5E-06	1,5E-03
ENSMUSG00000056592	Zfp658	Zinc finger protein 658	228,62	0,98	0,20	4,92	8,8E-07	1,0E-03

845
846

847

Table 1c. Cell types in wild type kidneys that expressed the genes differentially expressed in *Tshz3*$^{+/lacZ}$ kidney

Ensembl mouse ID	Mouse Gene symbol	Endothelium	Mesangium	Podocytes	Tubules	Immune
ENSMUSG00000054676	1600014C10Rik	X	X	X	X	
ENSMUSG00000086474	9130204K15Rik					
ENSMUSG00000004668	Abca13	X		X	**X**	
ENSMUSG00000031659	Adcy7			X		X
ENSMUSG00000004730	Adgre1					
ENSMUSG00000060470	Adgrg3	X		X	X	
ENSMUSG00000085180	Ai838599		X	X	X	
ENSMUSG00000033715	Akr1c14	X	X			
ENSMUSG00000028356	Ambp					
ENSMUSG00000020609	Apob					
ENSMUSG00000040694	Apobec2					
ENSMUSG00000020604	Arsg	X	X	X	X	
ENSMUSG00000038704	Aspdh					
ENSMUSG00000017929	B4galt5	X	X	X	X	X
ENSMUSG00000090486	BC035947					
ENSMUSG00000030268	Bcat1					
ENSMUSG00000058914	C1qtnf3					
ENSMUSG00000022416	Cacna1i					
ENSMUSG00000038128	Camk4			X	X	
ENSMUSG00000024610	Cd74	X		X		**X**
ENSMUSG00000022504	Ciita					

ENSMUSG00000056025	Clca3a1					
ENSMUSG00000040663	Clcf1	X		X	X	
ENSMUSG00000024330	Col11a2			X	X	
ENSMUSG00000030905	Crym			X		
ENSMUSG00000038642	Ctss			X		**X**
ENSMUSG00000027014	Cwc22	X	X	X	X	X
ENSMUSG00000015340	Cybb			X	X	X
ENSMUSG00000074254	Cyp2a4					
ENSMUSG00000108332	D530033B14Rik					
ENSMUSG00000031294	D630029K05Rik					
ENSMUSG00000025279	Dnase1l3					
ENSMUSG00000040658	Dnph1	X		X	X	
ENSMUSG00000020143	Dock2			X		
ENSMUSG00000025153	Fasn	X	X	X	X	
ENSMUSG00000003420	Fcgrt	X	X	X	X	X
ENSMUSG00000078650	G6pc	X	X	X	X	X
ENSMUSG00000033676	Gabrb3					
ENSMUSG00000040264	Gbp2b	X	X	X		
ENSMUSG00000079363	Gbp4	X		X	X	
ENSMUSG00000046352	Gjb2					
ENSMUSG00000066407	Gm10263	X	X	X	X	X
ENSMUSG00000087353	Gm13727					
ENSMUSG00000093006	Gm24157			X	X	
ENSMUSG00000098747	Gm27216					
ENSMUSG00000110631	Gm42047					

ENSMUSG00000104737	Gm42937	X		X	X	
ENSMUSG00000115154	Gm49067					
ENSMUSG00000111942	Gm5182					
ENSMUSG00000072324	Gm8420	X	X	X	X	X
ENSMUSG00000025534	Gusb	X	X	X	X	X
ENSMUSG00000036594	H2-Aa	X		X		**X**
ENSMUSG00000073421	H2-Ab1	X		X	X	**X**
ENSMUSG00000037649	H2-DMa		X	X	X	X
ENSMUSG00000067235	H2-Q10	X	X	X	X	X
ENSMUSG00000034551	Hdx	X	X	X		
ENSMUSG00000054072	Iigp1	X	X	X	X	
ENSMUSG00000000157	Itgb2l		X	X		
ENSMUSG00000058740	Kcnt1					
ENSMUSG00000063177	Klk1b27				X	
ENSMUSG00000028581	Laptm5	X		X		**X**
ENSMUSG00000022587	Ly6e	**X**	X	X	**X**	**X**
ENSMUSG00000069516	Lyz2			X		**X**
ENSMUSG00000012187	Mogat1					
ENSMUSG00000046805	Mpeg1			X		**X**
ENSMUSG00000022679	Mpv17l	X	X	X	X	
ENSMUSG00000019992	Mtfr2	X		X		
ENSMUSG00000038670	Mybpc2			X		
ENSMUSG00000001056	Nhp2	X	X	X	X	
ENSMUSG00000074151	Nlrc5	X	X	X		X
ENSMUSG00000029819	Npy	X	X	X	X	

ENSMUSG00000032690	Oas2					
ENSMUSG00000021913	Ogdhl					
ENSMUSG00000038910	Plcl2	X		X	X	X
ENSMUSG00000052160	Pld4			X		X
ENSMUSG00000042251	Pm20d1	X		X	X	
ENSMUSG00000030423	Pop4	X	X	X	X	X
ENSMUSG00000020684	Rasl10b					
ENSMUSG00000021876	Rnase4	X	X	X	X	
ENSMUSG00000031609	Sap30	X	X	X	X	X
ENSMUSG00000038224	Serpinf2					
ENSMUSG00000035699	Slc51a					
ENSMUSG00000025790	Slco3a1	X	X	X	X	X
ENSMUSG00000040693	Slco4c1					
ENSMUSG00000044349	Snhg11					
ENSMUSG00000096054	Syne1	**X**	X	X	X	X
ENSMUSG00000056296	Synpr					
ENSMUSG00000022218	Tgm1					
ENSMUSG00000044583	Tlr7	X		X		
ENSMUSG00000040883	Tmem205	X	X	X	X	X
ENSMUSG00000048572	Tmem252	X		X		
ENSMUSG00000010307	Tmem86a	X	X	X	X	
ENSMUSG00000016942	Tmprss6					
ENSMUSG00000043621	Ubxn10					
ENSMUSG00000031710	Ucp1					
ENSMUSG00000027962	Vcam1	X	X	X		

ENSMUSG00000056592	Zfp658		X	X

From the interactive online database at https://shiny.mdc-berlin.de/mgsca/.

Karaiskos, N. *et al.* A Single-Cell Transcriptome Atlas of the Mouse Glomerulus. *Journal of the American Society of Nephrology : JASN* **29**, 2060-2068 (2018).

850

Table 1d. Gene sets enriched in kidneys from wild-type (top) and *Tshz3*$^{+/lacZ}$ (bottom) adult mice.

Gene Sets enriched in WT								
NAME	SIZE	ES	NES	NOM p-val	FDR q-val	FWER p-val	RANK AT MAX	LEADING EDGE
HALLMARK_OXIDATIVE_PHOSPHORYLATION	192	0.21979448	3.5341222	0.0	0.0	0.0	3407 4	tags=85%, list=64%, signal=233 %
HALLMARK_XENOBIOTIC_METABOLISM	185	0.20220149	3.2691824	0.0	0.0	0.0	8038	tags=35%, list=15%, signal=41 %
HALLMARK_FATTY_ACID_METABOLISM	147	0.18565473	2.6469336	0.0	6.734007E +5	0.002	7584	tags=33%, list=14%, signal=38 %
Gene Sets enriched in *Tshz3+/lacZ*								
NAME	SIZE	ES	NES	NOM p-val	FDR q-val	FWER p-val	RANK AT MAX	LEADING EDGE
HALLMARK_MITOTIC_SPINDLE	196	-0.5266113	-8.769232	0.0	0.0	0.0	2221 6	tags=94%, list=41%, signal=160 %
HALLMARK_INTERFERON_GAMMA_RESPONSE	184	-0.51867735	-8.325257	0.0	0.0	0.0	1950 4	tags=88%, list=36%,

								signal=138 %
HALLMARK_G2M_CHECKPOINT	192	0	-7.6077356	0.0	0.0	0.0	20349	tags=86%, list=38%, signal=138 %
HALLMARK_EPITHELIAL_MESENCHYMAL_TRANSITION	191	-0.4679353	-7.484958	0.0	0.0	0.0	15995	tags=76%, list=30%, signal=109 %
HALLMARK_TNFA_SIGNALING_VIA_NFKB	194	-0.4516578	-7.4689045	0.0	0.0	0.0	21210	tags=85%, list=40%, signal=139 %
HALLMARK_INFLAMMATORY_RESPONSE	194	-0.4648554	-7.388191	0.0	0.0	0.0	20228	tags=84%, list=38%, signal=134 %
HALLMARK_E2F_TARGETS	194	-0.44707173	-7.359824	0.0	0.0	0.0	20349	tags=82%, list=38%, signal=132 %
HALLMARK_APICAL_JUNCTION	191	-0.43906716	-7.0284314	0.0	0.0	0.0	20347	tags=82%, list=38%, signal=131 %
HALLMARK_ALLOGRAFT_REJECTION	183	-0.43641797	-7.023872	0.0	0.0	0.0	21228	tags=83%, list=40%, signal=137 %
HALLMARK_UV_RESPONSE_DN	140	-0.4880429	-6.7432823	0.0	0.0	0.0	20254	tags=86%, list=38%, signal=138 %
HALLMARK_IL2_STAT5_SIGNALING	190	-0.41261196	-6.596804	0.0	0.0	0.0	24815	tags=87%, list=46%,

								signal=162 %
HALLMARK_MYOGENESIS	197	-0.39249557	-6.3807335	0.0	0.0	0.0	2368 3	tags=83%, list=44%, signal=148 %
HALLMARK_P53_PATHWAY	193	-0.38617578	-6.2882223	0.0	0.0	0.0	2383 3	tags=83%, list=44%, signal=149 %
HALLMARK_ESTROGEN_RESPONSE_EARLY	193	-0.38673815	-6.170295	0.0	0.0	0.0	2324 7	tags=82%, list=43%, signal=144 %
HALLMARK_KRAS_SIGNALING_UP	188	-0.37593746	-5.9241505	0.0	0.0	0.0	2299 3	tags=80%, list=43%, signal=140 %
HALLMARK_HYPOXIA	190	-0.358095	-5.8049035	0.0	0.0	0.0	2349 4	tags=79%, list=44%, signal=141 %
HALLMARK_COMPLEMENT	180	-0.36794096	-5.7306614	0.0	0.0	0.0	2771 7	tags=88%, list=52%, signal=182 %
HALLMARK_KRAS_SIGNALING_DN	187	-0.35026854	-5.5609736	0.0	0.0	0.0	2545 6	tags=82%, list=47%, signal=156 %
HALLMARK_INTERFERON_ALPHA_RESPONSE	88	-0.5092165	-5.549178	0.0	0.0	0.0	2027 9	tags=89%, list=38%, signal=142 %
HALLMARK_ESTROGEN_RESPONSE_LATE	190	-0.32073304	-5.2083893	0.0	0.0	0.0	2210 3	tags=73%, list=41%,

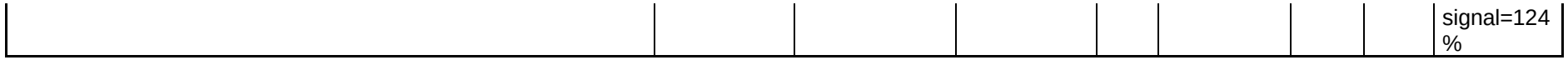
signal=124
%

853

Table 1e. ChIP enrichment analysis

Term	Overlap	Z-score	Combined Score	Genes
Interferon gamma signaling_Homo sapiens_R-HSA-877300	3/93	-1.79	11.67	CIITA;VCAM1;GBP4
Assembly of collagen fibrils and other multimeric structures_Homo sapiens_R-HSA-2022090	2/54	-2.03	9.92	COL11A2;CTSS
Interferon Signaling_Homo sapiens_R-HSA-913531	3/196	-2.08	9.26	CIITA;VCAM1;GBP4
Triglyceride Biosynthesis_Homo sapiens_R-HSA-75109	2/66	-1.98	8.93	MOGAT1;FASN
Collagen formation_Homo sapiens_R-HSA-1474290	2/85	-1.95	7.88	COL11A2;CTSS
Extracellular matrix organization_Homo sapiens_R-HSA-1474244	3/283	-1.99	6.94	VCAM1;COL11A2;CTSS
MHC class II antigen presentation_Homo sapiens_R-HSA-2132295	2/103	-1.85	6.80	CD74;CTSS
Lysine catabolism_Homo sapiens_R-HSA-71064	1/12	-1.66	5.92	CRYM
Endosomal/Vacuolar pathway_Homo sapiens_R-HSA-1236977	1/12	-1.51	5.39	CTSS
GABA A receptor activation_Homo sapiens_R-HSA-977441	1/13	-1.52	5.28	GABRB3

854
855

Table 1f. DEGs that are known direct targets of IRF8

Ensembl mouse ID	Mouse Gene symbol
ENSMUSG00000028356	Ambp
ENSMUSG00000020604	Arsg
ENSMUSG00000024610	Cd74
ENSMUSG00000022504	Ciita
ENSMUSG00000038642	Ctss
ENSMUSG00000015340	Cybb
ENSMUSG00000079363	Gbp4
ENSMUSG00000036594	H2-Aa
ENSMUSG00000073421	H2-Ab1
ENSMUSG00000037649	H2-DMa
ENSMUSG00000054072	Iigp1
ENSMUSG00000022587	Ly6e
ENSMUSG00000069516	Lyz2
ENSMUSG00000046805	Mpeg1
ENSMUSG00000032690	Oas2
ENSMUSG00000038910	Plcl2
ENSMUSG00000052160	Pld4
ENSMUSG00000030423	Pop4
ENSMUSG00000021876	Rnase4
ENSMUSG00000044583	Tlr7
ENSMUSG00000010307	Tmem86a
ENSMUSG00000056592	Zfp658

Table 1g. Human orthologs for differentially expressed genes

Human Gene symbol	Ensembl mouse ID	Mouse Gene symbol
C19orf12	ENSMUSG00000054676	1600014C10Rik
ABCA13	ENSMUSG00000004668	Abca13
ADCY7	ENSMUSG00000031659	Adcy7
ADGRE1	ENSMUSG00000004730	Adgre1
ADGRG3	ENSMUSG00000060470	Adgrg3
AMBP	ENSMUSG00000028356	Ambp
APOB	ENSMUSG00000020609	Apob
APOBEC2	ENSMUSG00000040694	Apobec2
ARSG	ENSMUSG00000020604	Arsg
ASPDH	ENSMUSG00000038704	Aspdh
B4GALT5	ENSMUSG00000017929	B4galt5
ERVW-1	ENSMUSG00000090486	BC035947
BCAT1	ENSMUSG00000030268	Bcat1
C1QTNF3	ENSMUSG00000058914	C1qtnf3
CACNA1I	ENSMUSG00000022416	Cacna1i
CAMK4	ENSMUSG00000038128	Camk4
CD74	ENSMUSG00000024610	Cd74
CIITA	ENSMUSG00000022504	Ciita
CLCF1	ENSMUSG00000040663	Clcf1
COL11A2	ENSMUSG00000024330	Col11a2
CRYM	ENSMUSG00000030905	Crym
CTSS	ENSMUSG00000038642	Ctss
CWC22	ENSMUSG00000027014	Cwc22
CYBB	ENSMUSG00000015340	Cybb
CYP2A13	ENSMUSG00000074254	Cyp2a4
DNASE1L3	ENSMUSG00000025279	Dnase1l3
DNPH1	ENSMUSG00000040658	Dnph1
DOCK2	ENSMUSG00000020143	Dock2
FASN	ENSMUSG00000025153	Fasn
FCGRT	ENSMUSG00000003420	Fcgrt
G6PC1	ENSMUSG00000078650	G6pc
GABRB3	ENSMUSG00000033676	Gabrb3
GBP3	ENSMUSG00000040264	Gbp2b
GBP6	ENSMUSG00000079363	Gbp4
GJB2	ENSMUSG00000046352	Gjb2
GUSB	ENSMUSG00000025534	Gusb
HLA-DQA1	ENSMUSG00000036594	H2-Aa
HLA-DQB1	ENSMUSG00000073421	H2-Ab1
HLA-DMA	ENSMUSG00000037649	H2-DMa

HLA-A	ENSMUSG00000067235	H2-Q10
HDX	ENSMUSG00000034551	Hdx
ITGB2	ENSMUSG00000000157	Itgb2l
KCNT1	ENSMUSG00000058740	Kcnt1
KLK3	ENSMUSG00000063177	Klk1b27
LAPTM5	ENSMUSG00000028581	Laptm5
LY6E	ENSMUSG00000022587	Ly6e
LYZ	ENSMUSG00000069516	Lyz2
MOGAT1	ENSMUSG00000012187	Mogat1
MPEG1	ENSMUSG00000046805	Mpeg1
MPV17L	ENSMUSG00000022679	Mpv17l
MTFR2	ENSMUSG00000019992	Mtfr2
MYBPC2	ENSMUSG00000038670	Mybpc2
NHP2	ENSMUSG00000001056	Nhp2
NLRC5	ENSMUSG00000074151	Nlrc5
NPY	ENSMUSG00000029819	Npy
OAS2	ENSMUSG00000032690	Oas2
OGDHL	ENSMUSG00000021913	Ogdhl
PLCL2	ENSMUSG00000038910	Plcl2
PLD4	ENSMUSG00000052160	Pld4
PM20D1	ENSMUSG00000042251	Pm20d1
POP4	ENSMUSG00000030423	Pop4
RASL10B	ENSMUSG00000020684	Rasl10b
RNASE4	ENSMUSG00000021876	Rnase4
SAP30	ENSMUSG00000031609	Sap30
SERPINF2	ENSMUSG00000038224	Serpinf2
SLC51A	ENSMUSG00000035699	Slc51a
SLCO3A1	ENSMUSG00000025790	Slco3a1
SLCO4C1	ENSMUSG00000040693	Slco4c1
SNHG11	ENSMUSG00000044349	Snhg11
SYNE1	ENSMUSG00000096054	Syne1
SYNPR	ENSMUSG00000056296	Synpr
TGM1	ENSMUSG00000022218	Tgm1
TLR7	ENSMUSG00000044583	Tlr7
TMEM205	ENSMUSG00000040883	Tmem205
TMEM252	ENSMUSG00000048572	Tmem252
TMEM86A	ENSMUSG00000010307	Tmem86a
TMPRSS6	ENSMUSG00000016942	Tmprss6
UBXN10	ENSMUSG00000043621	Ubxn10
UCP1	ENSMUSG00000031710	Ucp1
VCAM1	ENSMUSG00000027962	Vcam1

859

Table 1h. Human orthologues of DEGs that are associated with renal disease and/or autism spectrum disorder

Human Gene symbol	Kidney disease	reference	ASD	reference	Genetic syndromes that associate kidney conditions and ASD	reference
C19orf12						
ABCA13			YES	MalaCards, SFARI, AutDB		
ADCY7						
ADGRE1						
ADGRG3						
AMBP	Pyelonephritis, Urolithiasis, Hydronephosis, VUR 1, Hypertensive Nephropathy	MalaCards, DisGenet, AGR				
APOB	CKD, Nephrotic syndrome, Uremia,	MalaCards, AGR	YES	SFARI		
APOBEC2						
ARSG						
ASPDH						
B4GALT5						
ERVW-1						

BCAT1	Crescentic Glomerulonephritis	MalaCards				
C1QTNF3						
CACNA1I			YES	SFARI, AutDB		
CAMK4	Systemic Lupus Erythematosus, Kidney disease, Glomerulonephrititis, Focal Segmental Glomerulosclerosis	MalaCards	YES	SFARI, AutDB		
CD74	Renal Cell Carcinompa (nonpapillary), Kidney disease, Systemic Lupus Erythematosus, Polycystic Kidney Disease	MalaCards				
CIITA	Systemic Lupus Erythematosus, Tuberous Sclerosis 1	MalaCards, AGR	YES	MalaCards	Tuberous Sclerosis 1	Malacards
CLCF1						
COL11A2						
CRYM						
CTSS	Renal Cell Carcinoma	MalaCards				
CWC22						

CYBB	Renal Hypertension, Kidney Disease, ESRD, Renal fibrosis	MalaCards, DisGenet, AGR				
CYP2A13						
DNASE1L3	Systemic Lupus Erythematosus, Glomerulonephritis	MalaCards				
DNPH1						
DOCK2	Systemic Lupus Erythematosus,	MalaCards				
FASN	Kidney Cancer, ESRD, Renal Fibrosis	MalaCards, DisGenet				
FCGRT	Systemic Lupus Erythematosus	MalaCards				
G6PC1						
GABRB3	RETT Syndrome	MalaCards	YES	MalaCards, SFARI, DisGenet, AGR, AutDB	RETT Syndrome	MalaCards
GBP3						
GBP6						
GJB2	Horseshoe Kidney, Branchiootorenal Syndrome	MalaCards				

GUSB						
HLA-DQA1	Lupus Erythematosus, Nephrotic Syndrome, Tubulointerstitial Nephritis with Uveitis,	MalaCards, AGR				
HLA-DQB1	Systemic Lupus Erythematosus, Nephrotic Syndrome, PKD, Tubulointerstitial Nephritis with Uveitis	MalaCards				
HLA-DMA	Systemic Lupus Erythematosus, Membranous Nephropathy	MalaCards				

HLA-A	Systemic Lupus Erythematosus, CKD, Behcet Syndrome, Chronic Pyelonephritis, Wilms Tumor 5, Wilms Tumor 1, Renal Cell Carcinoma (nonpapillary), Membranous Nephropathy, Down Syndrome, Turner Syndrome, Nephrotic Syndrome, Kidney Cancer, ESRD, Uremia, Iga Glomerulonephritis,	MalaCards	YES	MalaCards, SFARI, DisGenet, AutDB	Down Syndrome	MalaCards
HDX	CKD, Kidney Disease, ESRD,	MalaCards				
ITGB2	Autoimmune Glomerulonephritis,	MalaCards				
KCNT1	Fragile X Syndrome	MalaCards	YES	AutDB	Fragile X Syndrome	MalaCards
KLK3	Urinary Tract Obstruction, Nephrogenic Adenoma, Hydronephrosis, Lower Urinary Tract Calculus, Chromophobe Renal Cell Carcinoma	MalaCards				

LAPTM5	Systemic Lupus Erythematosus	MalaCards				
LY6E						
LYZ						
MOGAT1						
MPEG1	Tafro Syndrome	MalaCards				
MPV17L	Chrmosome 16p13.3 Deletion Syndrome Proximal	MalaCards	YES	AutDB, AGR	Rubinstein-Taybi Syndrome	MalaCards, ClinVar
MTFR2						
MYBPC2						
NHP2						
NLRC5	Systemic Lupus Erythematosus, Renal Cell Carcinoma (nonpapillary), Renal fibrosis	MalaCards				
NPY	Turner Syndrome, Kidney Disease	MalaCards	YES	MalaCards		
OAS2						
OGDHL	PKD	MalaCards				
PLCL2						
PLD4	Nephrotic Syndrome (Type 7), Kidney Disease, CKD,	MalaCards				
PM20D1						
POP4						
RASL10B						

RNASE4						
SAP30	Renal Cell Carcinoma (Nonpapillary), Clear Cell Renal Celle Carcinoma	MalaCards				
SERPINF2						
SLC51A						
SLCO3A1						
SLCO4C1	CKD, Kidney Disease, PKD, Renal Oncocytoma	MalaCards, AGR				
SNHG11						
SYNE1			YES	SFARI, AutDB		
SYNPR						
TGM1						
TLR7	Systemic Lupus Erythematosus, Behcet Syndrome, Glomerulonephrititis, Turner Syndrome, Immune-Complex Glomerulonephritis	MalaCards				
TMEM205						
TMEM252						
TMEM86A						
TMPRSS6	Kidney Disease, CKD, ESRD	MalaCards				
UBXN10						

UCP1	Renal Cell Carcinoma (Nonpapillary),					
VCAM1	Systemic Lupus Erythematosus, Kidney Disease, Glomerulonephrititis,	MalaCards, AGR				

Abbreviations: ASD, Autism Spectrum Disorder; CKD, Chronic Kidney Disease; ESRD, End Stage Renal Disease; PKD, Polycystic Kidney Disease.

Data bases: MALACARDS (https://www.malacards.org); SFARI (https://gene.sfari.org); ClinVar (https://www.ncbi.nlm.nih.gov/clinvar/); DisGenet (https://www.disgenet.org);
AutDB (http://autism.mindspec.org/autdb/Welcome.do); AGR (Alliance of Genome Resources) (https://www.alliancegenome.org).

860
861

862

Table 1i. Detailed of proteins origin of the 33 differentially excreted urinary peptides obtained by the comparison between *Tshz3*$^{+/lacZ}$ heterozygous and WT control mice

PeptideID	p_value_BH	Masse	CE_t	Sequence	Prot_Name	Prot_Symbol	Prot_Accession	StartAA	StopAA	PeptideID	Mean LacZ	Mean WT	Mean LacZ/MeanWT	Fold-change
22340	0.012926897	1793,902	34,17476	EEASSTGRNFNVEKIN	Major urinary protein 17 (MUP 17)	MUP17	B5X0G2	19	34	22340	196,279666 7	2,16625	90,608	90,608
13942	0.016090788	1379,653	48,00482	EPGVTGLQGQAGPpG	Collagen alpha-1(VII) chain (Long-chain collagen) (LC collagen)	CO7A1	Q63870	1259	1273	13942	79,6890666 7	4,642083333	17,167	17,167
15681	0.025678503	1452,784	32,37929	ILGGQEAAAHARPY	Complement factor D (EC 3.4.21.46) (28 kDa adipocyte protein) (Adipsin) (C3 convertase activator) (Properdin factor D)	CFAD	P03953	26	39	15681	484,870666 7	30,8465	15,719	15,719
16620	0.029089955	1494,777	32,11926	SPGRHEAQEPFLQ	Tripeptidyl-peptidase 1 (TPP-1) (EC 3.4.14.9) (Lysosomal pepstatin-insensitive protease) (LPIC) (Tripeptidyl aminopeptidase) (Tripeptidyl-peptidase I) (TPP-I)	TPP1	O89023	293	305	16620	134,859866 7	16,183833 3	8,333	8,333
4260	0.041691443	1002,54	28,20322	KGEpGDTGVK	Collagen alpha-1(I) chain (Alpha-1 type I collagen)	CO1A1	P11087	815	824	4260	118,342666 7	16,583833 3	7,136	7,136
7480	0.033417318	1130,597	29,37694	ERIASEASRL	Histone H2B type 1-F/J/L (H2B 291A)	H2B1F	P10853	72	81	7480	387,188	55,476	6,979	6,979
19556	0.027812250	1646,898	28,02357	GEAGKPGRpGERGPpGP	Collagen alpha-1(I) chain (Alpha-1 type I collagen)	CO1A1	P11087	222	238	19556	77,3836	16,189583	4,780	4,780

12325	0.045781039	1315,638	38,83575	DGTpGGpGIRGMpG	Collagen alpha-1(III) chain	CO3A1	P08121	526	539	12325	410,4316	97,73	4,200	4,200
19711	0.041723205	1655,837	33,5862	GQPGAKGEpGDTGVKGDA	Collagen alpha-1(I) chain (Alpha-1 type I collagen)	CO1A1	P11087	810	827	19711	1149,643133	322,741083	3,562	3,562
972	0.027812250	859,4356	34,19798	GTAGEpGKAG	Collagen alpha-1(I) chain (Alpha-1 type I collagen)	CO1A1	P11087	576	585	972	193,0382667	56,17025	3,437	3,437
11936	0.012926897	1302,66	31,77936	GAKGEpGDTGVKGD	Collagen alpha-1(I) chain (Alpha-1 type I collagen)	CO1A1	P11087	813	826	11936	175,4740667	64,554666 7	2,718	2,718
21673	0.020169148	1759,903	34,0971	GRpGEVGPpGPpGPAGEKG	Collagen alpha-1(I) chain (Alpha-1 type I collagen)	CO1A1	P11087	906	924	21673	318,858933 3	119,334	2,672	2,672
931	0.033545397	857,4456	34,81086	INKEIQN	Clusterin (Apolipoprotein J) (Apo-J) (Clustrin) (Sulfated glycoprotein 2) (SGP-2) [Cleaved into: Clusterin beta chain; Clusterin alpha chain]	CLUS	Q06890	41	47	931	477,9655333	200,08875	2,389	2,389
7252	0.041723205	1122,567	36,71758	GPpGPpGAAGKEG	Collagen alpha-2(I) chain (Alpha-2 type I collagen)	CO1A2	Q01149	811	823	7252	1519,358133	679,16475	2,237	2,237
7194	0.036546003	1119,537	47,63876	GEVGPpGPpGPAG	Collagen alpha-1(I) chain (Alpha-1 type I collagen)	CO1A1	P11087	909	921	7194	4585,020267	2344,54742	1,956	1,956
7629	0.027812250	1136,51	47,73819	GQpGPpGPpGTAG	Collagen alpha-1(III) chain	CO3A1	P08121	329	341	7629	646,1975333	429,849167	1,503	1,503

8738	0.040602421	1180,583	37,838354	ApGEKGEGGPpGP	Collagen alpha-1(III) chain	CO3A1	P08121	828	840	8738	3789,516667	2618,54583	1,447	1,447
9385	0.018250194	1208,603	38,361833	ApGDRGEAGPpGP	Collagen alpha-1(I) chain (Alpha-1 type I collagen)	CO1A1	P11087	787	799	9385	11265,728	16686,7418	0,675	0,675
11018	0.036546003	1271,616	47,978442	GPpGPpGPpGPPSGG	Collagen alpha-1(I) chain (Alpha-1 type I collagen)	CO1A1	P11087	1170	1184	11018	1161,6598	2201,44125	0,528	0,528
19345	0.042316711	1636,828	40,732885	GSpGSpGPDGKTGPpGPAG	Collagen alpha-1(I) chain (Alpha-1 type I collagen)	CO1A1	P11087	531	549	19345	664,552733	1316,2705	0,505	0,505
9525	0.029758618	1214,591	47,907551	GPpGPpGpPGPSGP	Collagen alpha-1(XIII) chain	CODA1	Q9R1N9	277	290	9525	917,395866	1902,35583	0,482	0,482
8447	0.012926897	1168,609	37,4637	KpGEQGVPGDLG	Collagen alpha-1(I) chain (Alpha-1 type I collagen)	CO1A1	P11087	646	657	8447	2531,804933	5723,64083	0,442	0,442
15221	0.026816915	1433,725	38,808853	GEVGPpGPpGPAGEKG	Collagen alpha-1(I) chain (Alpha-1 type I collagen)	CO1A1	P11087	909	924	15221	784,599666	2096,30342	0,374	0,374
15447	0.045781039	1441,689	48,127044	GPPGPEGPpGPpGLQG	Collagen alpha-1(XIII) chain	CODA1	Q9R1N9	602	617	15447	658,7401333	1763,64717	0,374	0,374
14987	0.030131027	1421,719	39,359221	RGETGpAGpQGPpGP	Collagen alpha-1(XIV) chain	COEA1	Q80X19	1492	1506	14987	2405,853867	6710,77217	0,359	0,359

19285	0.011084765	1633,82	41,1177 4	EVGPpGPPGpAGEKGSpG	Collagen alpha-1(I) chain (Alpha-1 type I collagen)	CO1A1	P11087	910	927	19285	893,802866 7	4596,77767	0,194	0,194
19606	0.002681798	1649,815	41,2899 7	EVGPpGPpGpAGEKGSpG	Collagen alpha-1(I) chain (Alpha-1 type I collagen)	CO1A1	P11087	910	927	19606	1646,131467	9486,79592	0,174	0,174
13399	0.012926897	1357,649	31,5735 8	NGDDGEAGKpGRpG	Collagen alpha-1(I) chain (Alpha-1 type I collagen)	CO1A1	P11087	218	231	13399	583,4166667	3496,79808	0,167	0,167
19995	0.028818934	1671,65	48,0321 4	TGDSGPAGpPGPpGppGPP	Collagen alpha-1(I) chain (Alpha-1 type I collagen)	CO1A1	P11087	1160	1178	19995	881,218	6896,02167	0,128	0,128
7284	0.012926897	1123,553	36,2466 4	GGKGEQGPAGPpG	Collagen alpha-2(I) chain (Alpha-2 type I collagen)	CO1A2	Q01149	547	559	7284	85,35273333	893,795417	0,095	0,095
1502932	0.027812250	1520,763	40,0275 7	VGPpGPpGpAGEKGSpG	Collagen alpha-1(I) chain (Alpha-1 type I collagen)	CO1A1	P11087	911	927	150293 2	113,7734	1341,77408	0,085	0,085
8166	0.012926897	1157,543	47,7683 2	GPpGPpGPpGPpA	Collagen alpha-1(XV) chain [Cleaved into: Restin (Endostatin-XV)]	COFA1	O35206	1075	1087	8166	392,053333 3	4803,21583	0,082	0,082
21333	0.041723205	1741,984	34,2490 8	FIDQTRVLNLGPITR	Uromodulin (Tamm-Horsfall urinary glycoprotein) (THP) [Cleaved into: Uromodulin; secreted form]	UROM	Q91X17	593	607	21333	58,2154666 7	989,7535	0,059	0,059

p = hydroxylated proline

863
864

Abbreviations

B-Gal, Beta-Galactosidase

EnC, endothelial cell cytoplasm

F, endothelial fenestration

GBM, glomerular basement membrane

GEC, glomerular endothelial cells

HET, hererozygous

P: papilla

Po, podocyte foot process

SD, standard deviation

SEM, Standard Errors of the Mean

u: urothelium

WT, wild type